International Journal of Nanomedicine

Dovepress
open access to scientific and medical research

Open Access Full Text Article

ORIGINAL RESEARCH

RETRACTED ARTICLE: Mucus-Permeable Sonodynamic Therapy Mediated Amphotericin B-Loaded PEGylated PLGA Nanoparticles Enable Eradication of *Candida albicans* Biofilm

Min Yang[1,2], Mengyao Xie[1,2], Jiajun Guo[1,2], Yuqing Zhang[1,2], Yan Qiu[1,2], Zhibiao Wang[1,2], Yonghong Du[1,2]

[1]State Key Laboratory of Ultrasound in Medicine and Engineering, College of Biomedical Engineering, Chongqing Medical University, Chongqing, 400016, People's Republic of China; [2]Chongqing Key Laboratory of Biomedical Engineering, Chongqing Medical University, Chongqing, 400016, People's Republic of China

Correspondence: Zhibiao Wang; Yonghong Du, State Key Laboratory of Ultrasound in Medicine and Engineering, College of Biomedical Engineering, Chongqing Medical University, Chongqing, 400016, People's Republic of China, Tel/Fax +86-23-68485021; +86-23-68485021, Email wangzb@cqmu.edu.cn; duyonghong@cqmu.edu.cn

Background: *Candida albicans* (*C. albicans*) forms pathogenic biofilms, and the dense mucus layer secreted by the epithelium is a major barrier to the traditional antibiotic treatment of mucosa-associated *C. albicans* infections. Herein, we report a novel anti-biofilm strategy of mucus-permeable sonodynamic therapy (mp-SDT) mediated by ultrasound (US)-mediated amphotericin B-loaded PEGylated PLGA nanoparticles (AmB-NPs) to overcome the mucus barrier and enable the eradication of *C. albicans* biofilm.

Methods: AmB-NPs were fabricated using ultrasonic double emulsion method, and their physicochemical and sonodynamic properties were determined. The mucus and biofilm permeability of US-mediated AmB-NPs were further investigated. Moreover, the anti-biofilm effect of US-mediated AmB-NPs treatment was thoroughly evaluated on mucus barrier abiotic biofilm, epithelium-associated biotic biofilm, and *C. albicans*-induced rabbit vaginal infections model. In addition, the ultrastructure and secreted cytokines of epithelial cells and the polarization of macrophages were analyzed to investigate the regulation of local cellular immune function by US-mediated AmB-NPs treatment.

Results: Polymeric AmB-NPs display excellent sonodynamic performance with massive singlet oxygen ($^1O_2$) generation. US-mediated AmB-NPs could rapidly transport through mucus and promote permeability in biofilms, which exhibited excellent eradicating ability to *C. albicans* biofilms. Furthermore, in the vaginal epithelial cells (VECs)-associated *C. albicans* biofilm model, the mp-SDT scheme showed the strongest biofilm eradicative effect, with up to 98% biofilm re-formation inhibition rate, improved the ultrastructural damage, promoted local immune defense enhancement of VECs, and regulated the polarization of macrophages to the M1 phenotype to enhance macrophage-associated antifungal immune responses. In addition, mp-SDT treatment exhibited excellent therapeutic efficacy against *C. albicans*-induced rabbit vaginitis, promoted the recovery of mucosal epithelial ultrastructure, and contributed to the reshaping of a healthier vaginal microbiome.

Conclusion: The synergistic anti-biofilm strategies of mp-SDT effectively eradicated *C. albicans* biofilm and simultaneously regulated local antifungal immunity enhancement, which may provide a new approach to treat refractory drug-resistant biofilm-associated mucosal candidiasis.

Keywords: *C. albicans* biofilm, PEGylated nanoparticles, mucus penetration, sonodynamic therapy

Introduction

Candida albicans (*C. albicans*), a member of the mucosal flora of healthy people, is the most prevalent fungal pathogen in humans causing superficial mucosal fungal infection. Among them, the most typical and common colonization of *C. albicans* is vaginal mucosa and oral mucosa, resulting in vulvovaginal candidiasis (VVC) and oropharyngeal

Received: 20 September 2023
Accepted: 9 December 2023
Published: 27 December 2023

candidiasis (OPC), the most common forms of mucosal candidiasis.[1,2] A critical step toward fungal infection in superficial mucosa is the adhesion of *C. albicans* to mucosal epithelial cells and then inducing hyphal morphogenesis (transition between single-celled yeast cells to filamentous growth forms) and the expression of destructive secretases, such as aspartyl proteases and phospholipases, in the formation process.[3] Biofilms are microbial communities that attach to the surface of mucosa or biological materials embedded in a self-produced extracellular polymeric substance (EPS; major sugars, and proteins), which is a barrier structure with a self-protection function to evade the immune function of the host and prevent permeation of antibiotics. Moreover, biofilms have been verified to be closely associated with treatment failure and infection recurrence in mucosal-related *C. albicans* infections such as recurrent VVC.[3–5]

However, in *C. albicans* related mucosal infections, biofilm is not the only barrier that drugs must overcome before successful treatment. The mucus layer, as a natural physiological barrier, is a complex biological hydrogel that covers all wet epithelia in the body, including the oral cavity, respiratory, gastrointestinal, and vaginal tracts, which has evolved to protect the body from pathogenic infections, simultaneously, mucus also acts as an effective drug delivery barrier.[6] Mucins, as the main component of mucus, can physically and chemically interact with each other and with other components of mucus to form a mesh-like structure (average pore size 10–500 nm), which can limit drug penetration to the underlying epithelium by steric and/or adhesive interactions, especially those with cationic or hydrophobic properties.[7,8]

For mucosal candidiasis of VVC or OPC, transvaginal or oral localized drug delivery to mucosal surfaces is recommended as the first choice due to its low systemic side effects, but the existence of the mucosal barrier as mentioned above makes local delivery of traditional antibiotics face great challenges. Fortunately, nanoparticle-based delivery strategies are being explored and represent promising alternatives to promote the delivery of antibiotics into mucus-related bacterial biofilms.[9,10] Recently, a variety of surface-engineered nanoparticles have been developed to reduce the adhesive interaction of nanoparticles with mucus. Among them, low molecular weight polyethylene glycol (PEG) densely coated on the surface of nanoparticles can shield the nanoparticle core from adhesive interactions with mucus and help rapid diffusion of nanoparticles through human mucus, which may be a potential strategy to overcome the limitations of traditional nanoparticles in mucus delivery.[11,12]

Amphotericin B (AmB) is one of the most effective antifungal agents used to treat invasive fungal infections. However, the physicochemical properties of AmB, such as low solubility, tendency to self-aggregate in aqueous media, and low permeability, preclude its vaginal or oral topical delivery. So despite the versatility and importance of AmB in managing fungal infections, AmB is only used in very serious fungal infections via only intravenous injection.[13,14] However, the development of nanoparticle-mediated drug delivery system may provide the possibility to reduce drug toxicity and local application of AmB.[15] Previously, we demonstrated that AmB package loaded into poly(lactic-co-glycolic acid) (PLGA) nanoparticles can significantly reduce toxicity with good water solubility and dispersion, making it possible to deliver AmB locally for mucosal candidiasis treatment.[16] In addition, AmB or AmB loaded-nanoparticles may be activated by US to exert sonodynamic properties, which may be related to the fact that the maximum absorption peak of AmB (λ_{max} at 381, and 405 nm) is correlated well with the maximum emission of sonoluminescence in water (250–600 nm).

Sonodynamic therapy (SDT) is a promising combination therapy based on low-intensity ultrasound (US)-activated chemotherapeutic agents (sonosensitizer) to produce highly oxidative active reactive oxygen species (ROS) and ultimately achieve efficient bactericidal effect.[18] However, sonodynamic antimicrobial chemotherapy is not totally dependent on ROS-mediated toxicity, a sonophoresis phenomenon based on acoustic cavitation that can greatly enhance the permeability of skin and blood-brain barrier and increase the distribution of drugs in solid tissues.[19] In previous studies, we have demonstrated that ultrasound-mediated AmB-loaded nanoparticles can improve the efficiency of intravaginal drug delivery and play a highly effective antifungal role in in vitro plankton *Candida* and in vivo VVC infection.[20] However, how ultrasound-mediated nanoparticles penetrate the double barrier of mucus and biofilm, as well as the clearance effect of sonodynamic effects on the *Candida* biofilm associated with the epithelium under the mucus barrier and the local antifungal immunomodulation effect on cells remain unclear.

To date, the effect of the mucus layer on the treatment of mucosal candidiasis has often been ignored, and it is difficult to effectively cross the mucus and biofilm barrier to completely eliminate *C. albicans* in the biofilm. Herein, we

utilize a novel anti-biofilm strategy of mucus-permeable sonodynamic therapy (mp-SDT) based on low-intensity US-mediated PEGylated PLGA drug-loaded nanoparticles (AmB-NPs) to overcome both biofilm and mucus layer obstruction and enable the eradication of *C. albicans* biofilm (Figure 1). On the basis of the previous vaginal plankton *Candida* infection research, we further systematically investigated how this mp-SDT regimen improves drug delivery in mucus and biofilm obstruction in vitro and its significant anti-biofilm effect on mucus barrier abiotic biofilm, epithelium-associated biotic biofilm, and *C. albicans*-induced rabbit vaginal biofilms model, as well as its regulating effect on local cellular antifungal immune function.

Materials and Methods

Synthesis and Characterization of AmB-NPs

Amphotericin B-loaded PEGylated PLGA nanoparticles (AmB-NPs) were fabricated according to a slightly modified two-step ultrasonic emulsification method, as described previously.[16,21] A typical synthesis is as follows: $PLGA_{15k}$-PEG_{3k} powder (Daigang Biomaterial Co., China) was dissolved completely in dichloromethane (25 mg/mL, 2 mL) and mixed with AmB solution (5 mg/mL, 400 μL). Then, the polymeric mixture was subjected to ultrasonic emulsification at 150 W (50% duty ratio) for 2 min (work 5 s, interval 5 s) to obtain an initial water-in-oil (W/O) emulsion. Next, 4% PVA aqueous solution (4 mL) was added to the polymeric mixture and proceeded to produce a second ultrasonic oscillation for another 5 min to form water-in-oil-in-water (W/O/W) nanoemulsion formulations. Finally, the prepared AmB-NPs were purified by magnetic stirring (80–90 r/min) and triple centrifugation (10000 rpm,10 min) to remove any impurities. The yellowish AmB-NPs were re-suspended in distilled water and stored at 4°C until further use. $PLGA_{15k}$ nanoparticles were fabricated using the same procedure as that used for the controls. The morphological characteristics and stability of

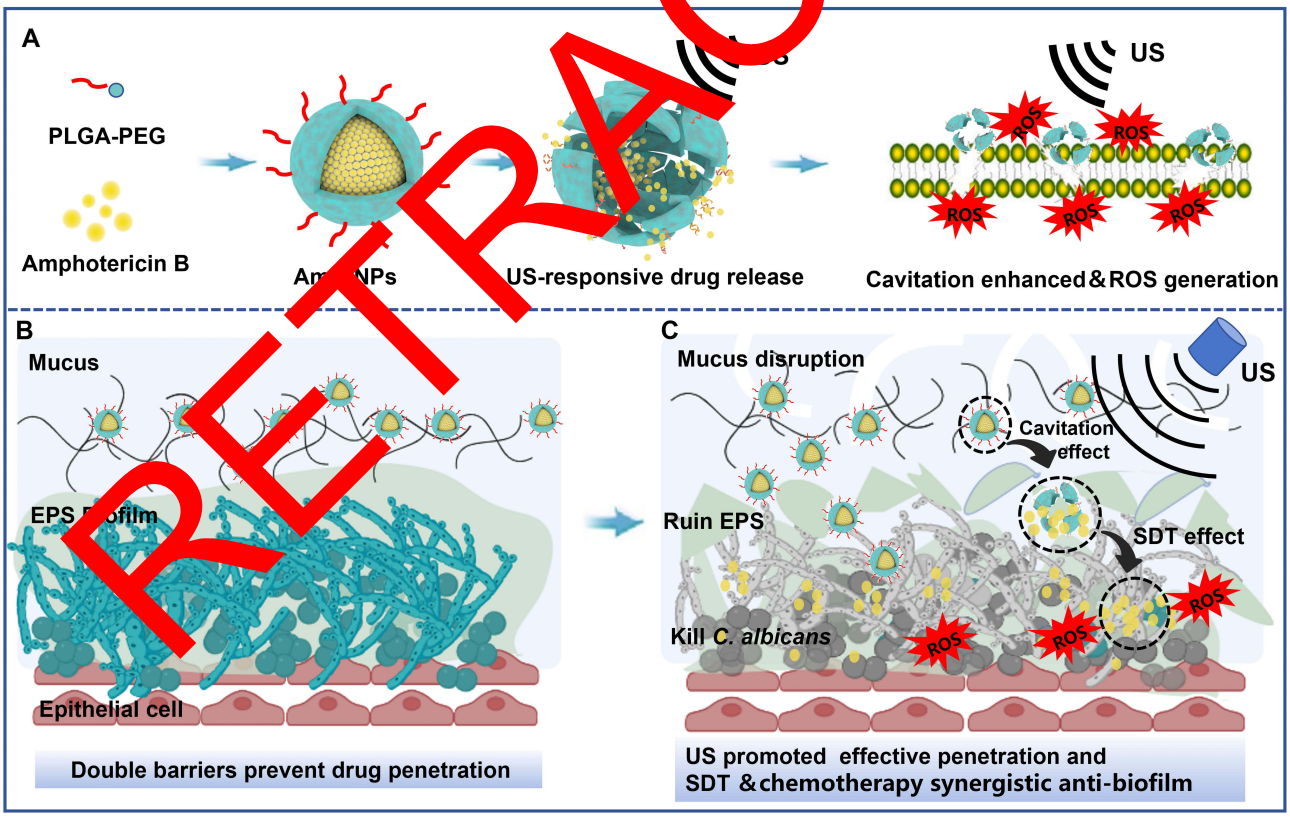

Figure 1 The schematic illustration of low intensity US-mediated PEGylated PLGA AmB-loaded nanoparticles (AmB-NPs) overcomes mucus barrier and eradicates of *C. albicans* biofilm.

Notes: (**A**) The synthesis of AmB-NPs and US-responsive drug release from nanoparticles, the enhancement of cavitation effect, and the production of ROS by ultrasound-mediated AmB-NPs. (**B**) The double barriers of mucus and biofilm EPS prevent drug penetration in the epithelium associated with *Candida* infection. (**C**) US-mediated AmB-NPs overcome both biofilm and mucus layer obstruction and effectively eradicates *C. albicans* biofilm under synergistic enhancement effect of SDT and chemotherapy.

the nanoparticles were determined by scanning electron microscopy (SEM, Hitachi S-3400N, Japan), transmission electron microscopy (TEM, Hitachi H-7600, Japan), and dynamic light scattering (DLS, Malvern Instruments, UK). The drug-loading content (LC%) and encapsulation efficiency (EE%) of AmB-NPs were analyzed using a UV–vis spectrophotometer (UV-2600 SHIMADZU, Japan) at 365 nm.

Detection of Sonodynamic Properties of AmB-NPs

The generation of singlet oxygen ($^1O_2$) was detected using a singlet oxygen sensor green kit (SOSG, Sigma, USA). Briefly, the SOSG probe (5 μM, 0.5 mL) was mixed with 2 mL of the free AmB and AmB-NPs solutions (4 μg/mL). Then the mixture was sonicated by a low-intensity US at an intensity of 1.0 W/cm^2 for 5 min (50% duty ratio). After sonication, the fluorescence intensity (FI) of SOSG was immediately detected using a fluorescence spectrophotometer at an excitation wavelength of 504 nm and emission wavelength of 525 nm. The same amount of PBS [illegible] subjected to sonication was used as the control. Subsequently, AmB-NPs and AmB were sonicated for diffe[illegible]nt duration[illegible] to explore the influence of ultrasonic dose on $^1O_2$ production. The experiments were independently repeat[illegible] three time[illegible]

Microbial Strains and Cell Culture

The standard strain, ATCC 10231 *C. albicans* was provided by the China Gen[illegible]al M[illegible]biologica[illegible] Culture Collection Center. The cryopreserved fungal solution was inoculated into Sabouraud De[illegible]se broth (H[illegible]nk[illegible] Microbial Co., China) at 37°C for 24 h with agitation at 150 rpm, cells were then harvested, [illegible]nd re[illegible]spended in Roswell Park Memorial Institute 1640 (RPMI, Gibco, USA) medium containing 10% fetal [illegible]ovine seru[illegible] (FBS, Gibco, USA) for biofilm formation.

Human vaginal epithelial cells (VECs) of VK2/E6E7 (Bio-[illegible]8277, Beiji[illegible] Biobw Biotechnology Co. LTD) and macrophages (RAW264.7, Shanghai Institute of Cell Research[illegible] Chinese A[illegible]ademy of Sciences) were cultured in Dulbecco's modified Eagle's medium (DMEM, Gibco, [illegible]SA) supple[illegible]nte[illegible] with penicillin (100 U/mL), streptomycin (100 mg/L), and 10% FBS at 37°C in a 5% CO_2 incuba[illegible]r.

Mucus and Biofilms Permeability Stud[illegible] of U[illegible]S-Mediated Nanoparticles

Particle-Mucin Binding Assay

In this study, DiI fluorescent-labelled [illegible]nopar[illegible]s (DiI-NPs, 20 μg/mL) were used as a model to study the permeability of US-mediated nanoparticles in m[illegible]s and biofi[illegible]s. To measure particle-mucin aggregates, PLGA DiI-NPs and PLGA-PEG DiI-NPs were mixed with [illegible]ucin [illegible]lution (10 mg/mL, Sigma, USA) in a cell culture dish, which was then subjected to ultrasonic irradiation at t[illegible] bottom of th[illegible]ulture plate at an intensity of 1.0 W/cm^2 for 5 min, as described previously. After 3 h of incubation [illegible]th a sp[illegible]ed of 100 rpm at 37°C, the supernatant was collected by centrifugation (3000 rpm, 5 min) to measure FI o[illegible] DiI in [illegible] fluorescence spectrophotometer. Nanoparticles-mucin aggregation rate was calculated using the equati[illegible][10] Ag[illegible]egation[illegible]e% = $(FI_0 - FI_1)/FI_0 \times 100\%$ (FI_0 is the fluorescence intensity of DiI before incubation, F[illegible] is the [illegible]uresc[illegible] intensity of DiI in the supernatant after incubation).

Distribution [illegible]anoparticles in Simulated Vaginal Mucus

To observe the sp[illegible]ific distribution of nanoparticles in mucus after sonication, a simulated vaginal mucus (SVM) was developed using the [illegible]ethod previously described by Owen and Katz.[22] The SVM was composed of 1.0 g acetic acid, 0.018 g bovine serum albumin, 0.222 g $Ca(OH)_2$, 0.6 g glycerol, 5.0 g glucose, 1.4 g KOH, 2.0 g lactic acid, 3.51 g NaCl, and 0.4 g urea in 1 L of distilled water, which had a similar viscosity to mid-cycle cervicovaginal fluid. The SVM was adjusted to pH 7.0 by adding 0.1 N NaOH solution to simulate the environment found in the case of vaginal infection.[23] Then, PLGA DiI-NPs and PLGA-PEG DiI-NPs were added to the SVM in the culture plates, and ultrasonic irradiation was then performed at an intensity of 1.0 W/cm^2 for 5 min at the bottom of culture plate. After irradiation and static reaction for 2 h at room temperature, the infiltration and distribution of DiI-NPs (red fluorescence) into the mucus was observed using a laser scanning confocal microscope (LSCM, Nikon, Japan), and the average area of DiI in the top, middle, and bottom layers of the mucus was calculated using five randomly selected view fields per layer.

Biofilm Permeation Analysis Under the Mucus Barrier

C. albicans (100 μL, 3.0×10^8 CFU/mL) was inoculated on transwell inserts with polycarbonate membranes (3 μm pore size) to form mature biofilms after 48 h of inoculation. Then, 100 μL of SVM was placed on the biofilms, and 100 μL of DiI-NPs were gently added onto the surface of the mucus to construct a double barrier model of mucus-coated biofilms. The upper chamber was inserted into the bottom chamber (contained 0.8 mL PBS), and the plate was immediately irradiated at an intensity of 1.0 W/cm^2 for 5 min at the bottom of the culture plate. Then, the bottom chamber samples were individually collected after 24 h incubation at a speed of 100 rpm at 37°C to detect FI of DiI and calculate the cumulative permeation using the following equation: Cumulative rate % = FI_1 / $FI_0\times100\%$ (FI_0 is the initial fluorescence intensity of DiI in the upper chamber, FI_1 is the fluorescence intensity of DiI in the bottom chamber). Subsequently, the *C. albicans* biofilms were labeled with calcium fluorescent white (CFW; Sigma), and the infiltration and distribution of DiI-NPs in the top, middle, and bottom layers of the biofilm were observed using LSCM scanning with a layer spacing of 2 μm.

In vitro Cellular Uptake of Nanoparticles Assay Under the Mucus Barrier

To explore whether US can affect the cellular uptake of nanoparticles in the presence of the mucus barrier, VK2/E6E7 cells were placed in a VWR 35-mm confocal dish (1×10^6 cells each) and attached to the dish after overnight culture. The medium was then replaced with 500 μL of SVM (diluted with DMEM) containing DiI-NPs (200 μL NPs per dish), and the plate was irradiated immediately at an intensity of 1.0 W/cm^2 for 5 min at the bottom of the culture plate. After sonication, the plate was continuously incubated for 2, 6, and 24 h. Subsequently, the cells were washed twice with cold PBS to remove complexes that were not taken up, and the nuclei were stained with 4,6-diamidino-2-phenylindole (DAPI, Beyotime) for cellular uptake of nanoparticles using CLSM. In addition, the cells were re-suspended in PBS (0.5 mL), and the cellular uptake rate of the nanoparticles was further verified quantitatively using a flow cytometer (FC500, BD Biosciences).

Anti-Biofilm Effect of US-Mediated AmB-NPs in Mucus Barrier Biofilm Model

Constructed Mucus Barrier Biofilm Model and Grouped Treatment

Mature *C. albicans* biofilms were developed on 24-well plates after 48 h of incubation, and 200 μL PBS was added just enough to touch the bottom of the Transwell insert membrane. Sterile transwell inserts were then placed on top of the biofilms, and 50 μL of sterilized SVM was placed on top of the transwell inserts. A mucus barrier biofilm model was constructed and subjected to the following treatments: 1) control (no drug, no US, only PBS); 2) US; 3) free AmB (only AmB); 4) US combined with free AmB (US+AmB); 5) AmB-NPs; and 6) US combined with AmB-NPs (US+AmB-NPs). Sterilized AmB-NPs and free AmB solution at final equivalent AmB concentrations of 4 μg/mL were added to the surface of the mucus, and the bottom of the plates was irradiated immediately at an intensity of 1.0 W/cm^2 for 5 min, as described previously. After the treatment was completed, the cells were incubated for another 24 h.

Evaluation of Biofilm Biomass, Viability, and Ultrastructure

The transwell inserts were removed and biofilms were rinsed and stained with 1% (w/v) crystal violet solution for 30 min, after which 1 mL of 33% acetic acid solution was added for decolorization and the biofilm biomass of different groups was determined by measuring the absorbance at 570 nm using a microplate reader. Then, LIVE/DEAD BacLight Bacterial Viability (Invitrogen, CA) were used to evaluate the viability of fungi in biofilms and simultaneously observe the biofilm architecture. The biofilm was stained with a mixture of SYTO 9 (stained live cells) and propidium iodide (PI, stained dead cells) solution at room temperature in the dark for 30 min. The stained biofilm was scanned using CLSM with a z-step size of 2 μm to reconstruct a 3D image of the biofilm. Live and dead fungi in the biofilm after treatment were calculated using green and red FI using ImageJ (National Institute of Health, USA). In addition, the overall morphology of the biofilm under mucus and the ultrastructural changes of mycothalli in the biofilm were observed using SEM.

Evaluation of Biofilm EPS

After 24 h of incubation following the experimental treatment, the EPS of the biofilm was stained with FITC-conA (500 μg/mL, Sigma) for 30 min in the dark, followed by observation using CLSM at an excitation wavelength of 488 nm and emission wavelength of 525 nm. The protein and polysaccharide contents in the EPS were determined using

bicinchoninic acid protein assay kits and the phenol-sulfuric acid method, respectively.[10] Briefly, EPS was first extracted from the biofilm by ultrasonication (60 W, 4 min) and centrifugation (11,000 × g, 45 min), and the supernatant was filtered through a 0.22 μm membrane. To determine polysaccharides, the purified EPS sample (90 μL) was mixed with 5% phenol solution (90 μL) and sulfuric acid (300 μL) in water bath at 90°C for 1 h incubation. The polysaccharide content was determined by measuring the absorbance at 490 nm, and the protein concentration was determined using a BCA assay kit (Beyotime, China) at 562 nm, according to the manufacturer's guidelines. The contents of polysaccharide and protein in treated biofilms were normalized to control (100%).

Analysis of Biofilm Hypoxia Changes

Image-iT™ Red Hypoxia Reagent (Invitrogen, CA) contains live-cell permeable compounds, which increase fluorescence in environments with low oxygen concentrations. *C. albicans* biofilm was grown on cell plates for 3 days as described previously using 500 μL of adjusted fugal suspension under mucus conditions. At 12, 24, 48, and 72 h, the hypoxy probe (10 μM, 100 μL) was added into the *C. albicans* biofilm for 60 min staining and simultaneously the *C. albicans* biofilms profile was labeled with CFW for 30 min to observe the changes of hypoxia environment during biofilm formation process. Next, to explore the hypoxia changes of internal biofilm after US-mediated AmB-NPs therapy, the biofilm was washed with PBS and labeled with Image-iT™ hypoxy probe to observe LSCM scanning with a layer spacing of 2 μm and then measured red/blue fluorescence area to reflect hypoxia range of different groups.

Quantification of ROS in Biofilm

The total intracellular ROS within the biofilm was first analyzed using a 2′,7′-dichlorodihydrofluorescein diacetate (DCFH-DA, Sigma) reagent kit. Prior to experiments, the biofilms were rinsed and supplemented with a fresh culture medium containing DCFH-DA (1 μM) at 37°C for 30 min to load probe. After 2 h of incubation following the experimental treatment described above, *C. albicans* biofilms were rinsed and stained with CFW. Intracellular ROS within the biofilm was observed using CLSM at wavelength of 495 nm (excitation) and 529 nm (emission). In addition, three representative types of ROS were detected using dihydroethidium (DHE), 30-(p-hydroxyphenyl) fluorescein (HPF), and SOSG probes, which are reagents that monitor superoxide anion (O_2^-), hydroxyl radical (·OH), and singlet oxygen ($^1O_2$) generation, respectively. After the biofilm treatment, the different methods and incubation for another 2 h, the biofilm was repeatedly dispersed with a pipette and suspended in PBS, and *C. albicans* suspension was stained with DHE and HPF for 30 min at 37°C. An SOSG probe was used to detect $^1O_2$ in an aqueous solution of the reaction system. After staining and reflection, the FI of each reagent was analyzed using a spectrophotometer.

Anti-Biofilm Ability in Mucus Simulated Epithelial Cell Biotic Biofilms Model

Analysis of *C. albicans* Adhesion to VK2/E6E7 Cells

Candida adhesion, infiltration and biofilm formation on the cell surface were observed in a VK2/E6E7 epithelial cell and *C. albicans* co-culture model. Briefly, VK2/E6E7 cells were incubated in a confocal plate (1×10^6 cells/well) and mixed with SYTO 9-labeled *C. albicans* (ratio of bacteria/cells: 1:100). *C. albicans* adhesion and invasion of epithelial cells was observed after 2, 6, 12, and 24 h of continuous culture. After that, to evaluate whether US- mediated AmB-NPs could inhibit adhesion of *C. albicans* to the cell biotic surface, the sterilized AmB-NPs and free AmB were re-suspended in serum-free medium solution containing 10% SVM at final equivalent AmB concentrations of 4 μg/mL and added to the plates. The bottom of the plates were irradiated immediately at a US intensity of 1.0 W/cm^2 for 5 min as described previously. After the treatment was completed, the cells were incubated for another 6 h. Finally, cells were labeled with DAPI and *C. albicans* adhesion to VK2/E6E7 cells in different treatments was observed by CLSM and detected by flow cytometry to quantitatively analyze the *C. albicans*-cell adhesion rate in each group.

Elimination of *C. albicans* Biofilm Formed on VK2/E6E7 Cells Surface

To further evaluate whether US-mediated AmB-NPs could effectively eliminate *C. albicans* biofilm formed on the biotic surface of VK2/E6E7 cells, DAPI-labeled cells were infected with 200 μL SYTO 9-labeled *C. albicans* for 24 h to form a mature *C. albicans* biofilm on the cell surface. After 24 h of incubation following 1) to 6) experimental treatment, the

elimination of *C. albicans* biofilm formed on the VK2/E6E7 cell surface was observed by CLSM. The survival of *C. albicans* colony in the biofilm was estimated by plating serially diluted cultures on SDA plates, and colony-forming units (CFUs) were counted after 48 h. After that, cells and *C. albicans* were collected and re-suspended in RPMI 1640 medium containing 10% FBS, and the re-suspended solution was added to a 96-well plate and continued to culture for 48 h. Crystal staining was used to observe the biofilm formation in the wells to analyze the biofilm re-formation rate.

Observation of Cell Ultrastructure Changes by TEM

After treatment for 24 h, the cells and *C. albicans* were washed, collected, and then fixed in 3% glutaraldehyde for 24 h at 4°C. After treatment, the cell samples were cut into ultrathin sections and then double-stained with 5% uranyl acetate and lead citrate. Subsequently, internal ultrastructural changes in epithelial cells and adherence and invasiveness of *C. albicans* in different groups were observed using TEM.

Cytokine Analysis by Enzyme-Linked Immunosorbent Assay

For the changes in the secretion changes of epithelial cell-associated cytokines after different treatments, the co-culture supernatants were collected, centrifuged (12,000g, 5 min), and stored at −80°C. The expression of interleukin 2 (IL-2), IL-4, IL-10, and IL-17 in the supernatant samples was determined using enzyme-linked immunosorbent assay (ELISA) test kits (Jingmei, China) according to the manufacturer's instructions. The absorbance values and concentrations of each cytokine were read with a 490 nm filter using a Ceres 900 automated microplate reader (BioTek Corp., Winooski, VT, USA). Each independent experiment was performed in triplicate.

Analysis of Macrophage-Associated Antifungal Immune Responses

Phagocytosis of Macrophages on the *C. albicans* Under Sonication

To study the phagocytic effect of macrophages on *C. albicans* under sonication, the RAW264.7 cells were inoculated in 6-well plates and mixed with FITC-labeled *C. albicans* at a ratio of 1:10, and then irradiated immediately with an intensity of 1.0 W/cm^2 for 150s, 300s, and 450s at the bottom of culture plate. Those cells without ultrasonic irradiation were used as the control. After co-incubation for another 4 h, the plates were washed three times and the RAW264.7 cells were stained with DAPI for phagocytosis observation by CLSM. Subsequently, flow cytometry was used for the quantitative analysis of phagocytosis.

Effect of Macrophage Polarization Under US-Mediated AmB-NPs Treatment

RAW264.7 macrophages (1×10^6) were incubated with FITC-labeled *C. albicans* at a ratio of 1:10 to stimulate the macrophages in an inflammatory state. LPS (1 μg/mL, Sigma) or IL-4 (50 ng/mL, Sigma) was added to each well for 24 h to induce the polarization of M1 and M2 macrophages, respectively. After 24 h incubation following 1) to 6) experimental treatment, the primary antibodies against CD86 and CD206 (Affinity, China) were added to each sample and incubated in the dark at 4°C overnight. After removal of the primary antibody, the samples were incubated with Cy5 fluorescein-labeled goat anti-rabbit secondary antibody for 60 min at room temperature, and the cells were stained with DAPI for 10 min. Finally, the M1/M2 phenotype inflammatory response of RAW 264.7 was observed using CLSM at wavelengths of 346 nm (excitation) and 664 nm (emission). In addition, cell supernatants were collected to detect M1 and M2 macrophage-associated markers (IL-1β, TNF-α, IL-10, and TGF-β) using ELISA, as described above.

In vivo Evaluation of Antifungal Efficacy in Vaginal *C. albicans* Biofilms Model

All animal experiments were carried out according to the guidelines of the China Laboratory Animal Guideline for Ethical Review of Animal Welfare (GB/T35892-2018) and approved by the Experimental Animal Ethics Committee of Chongqing Medical University (approval number: 2022162). The in vivo antifungal efficacy of the US-mediated AmB-NPs was evaluated in rabbit vaginal *C. albicans* biofilms model. Healthy rabbits were subcutaneously injected with 0.2 mL of estradiol benzoate injection (2 mg/mL) once daily for 3 days. On the fourth day, 100 μL of pre-cultured *C. albicans* biofilm solution was injected into the vagina with a pipette gun once a day for 3 days, and the rabbits were fed normally for another 1 day. Infected rabbits were intravaginally injected with 200 μL of saline, pure AmB (1 mg/mL), and AmB-NPs (20 mg/mL, equivalent to a pure AmB concentration of 1 mg/mL) solution, and then immediately

performed intravaginal US irradiation by a tubular annular transducer immediately at an intensity of 1.0 W/cm^2 for 5 min with a 50% duty cycle for 3 consecutive days treatment. On the third day after treatment completion, vaginal lavage fluid was collected for quantitative analysis of *C. albicans* cell viability and vaginal microbiome analysis using 16S rRNA gene sequencing. All groups of rabbits were euthanized, and vaginal tissues were collected for histopathological analysis using H&E staining and TEM.

Statistical Analysis

Statistical analyses in the present study were performed using GraphPad Prism 8.0 software (GraphPad Software, CA, USA). All data are presented as mean ± standard deviation (SD). The significance of the differences between two groups was determined using a two-tailed Student's *t*-test, and comparisons among multiple groups were performed using one-way ANOVA. Statistical significance was set at $P < 0.05$.

Results and Discussion

Physicochemical Characterization and Sonodynamic Properties of AmB-NPs

Physicochemical characterization and sonodynamic properties of the AmB-NPs copolymer are shown in Figure 2. SEM analysis revealed that the prepared AmB-NPs had a spherical shape, uniform size, good dispersion, and no obvious adhesion or local agglomeration (Figure 2A), with a consistent core-shell sphere observed under TEM (Figure 2B) and US-responsive drug release (Figure 2C). AmB-NPs exhibited a mean diameter of 252.25±4.5 nm with a polydispersity index (PDI) of 0.091±0.03 and a zeta potential of −22.0±0.78 mV, both of which had a narrow size distribution (Figure 2D and E). The physical properties of the nanoparticles themselves are crucial to prevent them from becoming trapped in mucus. Studies have shown that the particle diameters between 200 and 300 nm of these mucoadhesive formulations presented better characteristics to get through the mucus and bind to mucosal tissues.[24] The favorable size and negative surface charge of AmB-NPs are conducive for NPs to avoid electrostatic absorption and are trapped by mucus. Moreover, the size and charge value of AmB-NPs remained relatively consistent under physiological conditions for extended periods (Figure 2F and G), indicating the high stability of AmB-NPs and the possibility of further applications in in vivo treatment. The EE% and DLC% of AmB in AmB-NPs were 84 ± 1.5% and 5.1±0.18%, respectively.

Then, to ensure the SDT application of US-mediated AmB-NPs for biofilm treatment, the sonodynamic properties of AmB-NPs were investigated by assessing $^1O_2$ production. After ultrasonic irradiation, AmB and AmB-NPs solutions (4 μg/mL) both showed obvious $^1O_2$ fluorescence, and the FI of $^1O_2$ in ultrasonic interaction with AmB-NPs was higher than that of AmB (Figure 2H), indicating that loading drugs into the nanospheres may amplify the effect of SDT. In addition, the FI of $^1O_2$ is ultrasonically dose-dependent with the extension of irradiation time, but a single ultrasonic irradiation did not result in obvious $^1O_2$ production (Figure 2I). $^1O_2$ production proves that AmB or AmB-NPs can be activated by US to exert sonodynamic properties, which is attributed to a good overlap between the peak absorbance of AmB and the emission range of sonoluminescence, similar to both ciprofloxacin (λmax at 276, 316, and 328 nm) and levofloxacin (λmax at 288 and 331 nm)-mediated sonodynamic effects.[17,25]

US-Mediated Nanoparticles Promoted Mucus Penetration

Mucus, as an adhesive, viscoelastic gel is the first-line defense that covers all mucosal surfaces and effectively traps many pathogens, as well as antifungal agents. Mucin-nanoparticle aggregates can be used to predict the penetration ability of nanoparticles in mucus, and reduced binding with mucin is usually correlated with more rapid penetration through mucus.[11,26] The binding rates of PLGA DiI-NPs or PEGylated PLGA DiI-NPs to gastric mucin solution with or without sonication were comparatively measured. As shown in Figure 3A, PLGA NPs showed the highest aggregation rate (76.4%), followed by 52.8% of PEGylated NPs, while after US irradiation, the aggregation rate of PLGA NPs and PEGylated NPs were significantly decreased to 45.1% and 30.3%, respectively. The specific distribution of the nanoparticles in the mucus after sonication was observed using CLSM. Only weak DiI-red fluorescence was evident in the PLGA NPs group, while the fluorescence was somewhat stronger in the PEGylated NPs group and was markedly stronger in the PLGA-PEG NPs+US group, with clear red DiI fluorescence mainly distributed in the middle and bottom

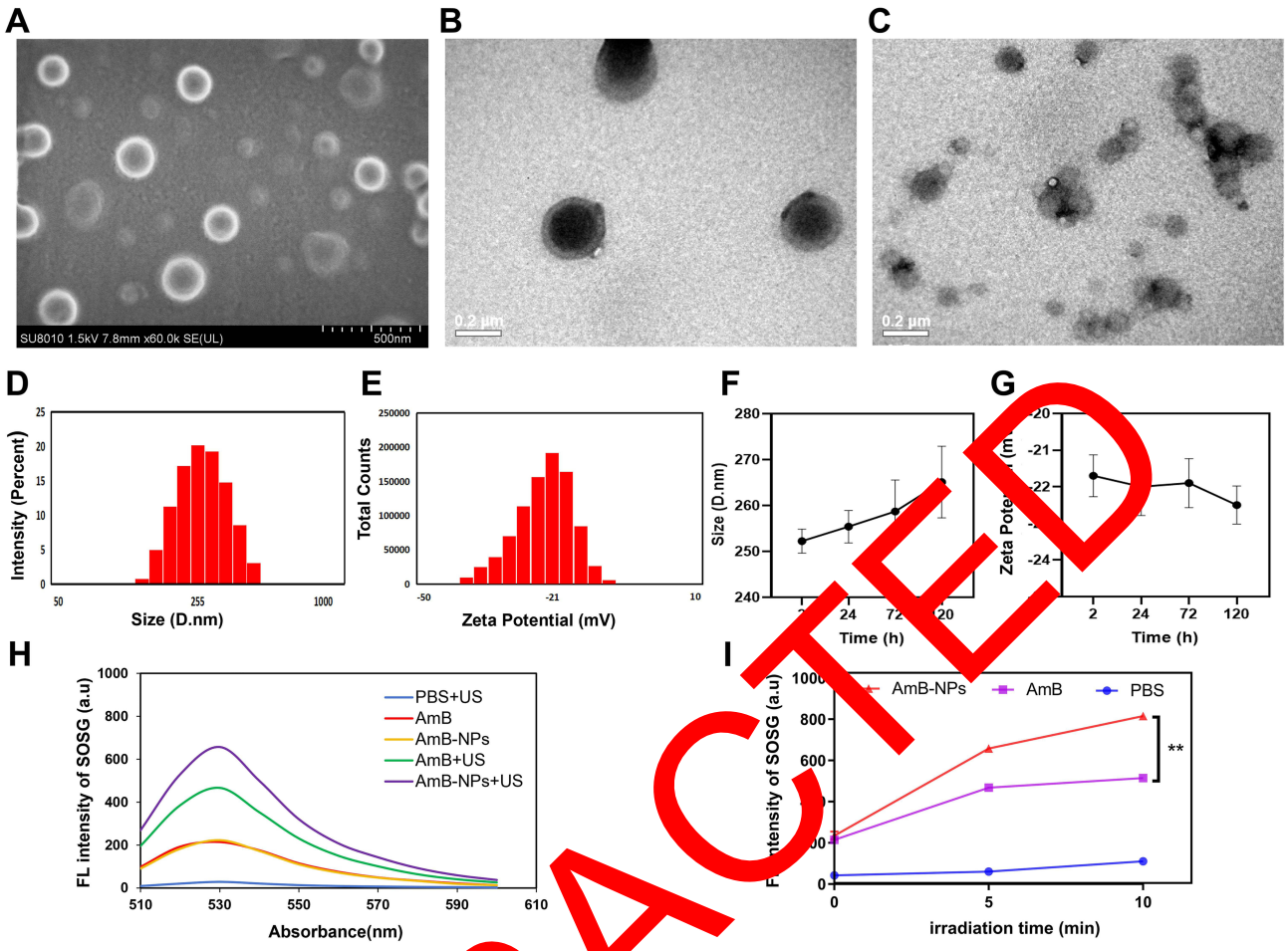

Figure 2 Characterization of the fabricated AmB-NPs.
Notes: (**A**) SEM image of AmB-NPs (scale bar = 500 nm). (**B**) TEM image of AmB-NPs (scale bar = 200 nm). (**C**) TEM Image of AmB-NPs under US irradiation (scale bar = 200 nm). (**D**) Size and (**E**) Zeta potential distribution of AmB-NPs for stability measurement. (**F**) Size and (**G**) Zeta potential distribution in 120 h for stability measurement of AmB-NPs. (**H**) The sonodynamic property of AmB-NPs was detected by assessing $^1O_2$ production. (**I**) $^1O_2$ content of AmB-NPs and AmB produced by ultrasonic irradiation at different times. The data are shown as mean ± SD, n = 3. $^{**}P < 0.01$.

layers of the mucus (Figure 3B). Further quantitative calculation of the amount of fluorescence in each layer of mucus showed that the average fluorescence intensity in the PLGA-PEG NPs+US group was significantly higher than that in the other groups, with a 6–10 fold increase relative to the PLGA NPs group and a 3–5 fold increase relative to the PLGA-PEG NPs group ($P < 0.01$) (Figure 3C). This result was in accordance with previous studies showing that PEGylated PLGA nanoparticles penetrate mucus more easily than unmodified nanoparticles.[11] More importantly, US can further improve the permeability of mucus, which may be related to the high shear force formed by the ultrasonic cavitation process. Under shear force, the viscosity of mucus can be reduced 100–1000 times close to the viscosity of water.[27]

US-Mediated Nanoparticles Improved Sub-Mucus Biofilm Penetration Enhancement

Mucus and biofilm structure are two barriers that antifungal drugs must break through in the treatment of mucosa-associated *Candida* infection.[5] The SVM is employed due to similarity of rheological and viscosity properties to mid-cycle cervicovaginal mucus.[28] The permeability of US-mediated nanoparticles through double barrier of mucus and biofilm was further evaluated and the schematic diagram as shown in Figure 4A. We visualized the transport of nanoparticles through a double barrier and the distribution of DiI-NPs in the biofilm after 24 h of incubation using CLSM (Figure 4B). Notably, PLGA-PEG NPs+US treatment resulted in a large number of red fluorescent particles mainly distributed deep inside the biofilm. However, the red fluorescence particle distribution at the bottom of the biofilm was not obvious in the other groups. The cumulative permeation (%) of DiI-NPs from the apex of the donor chamber to

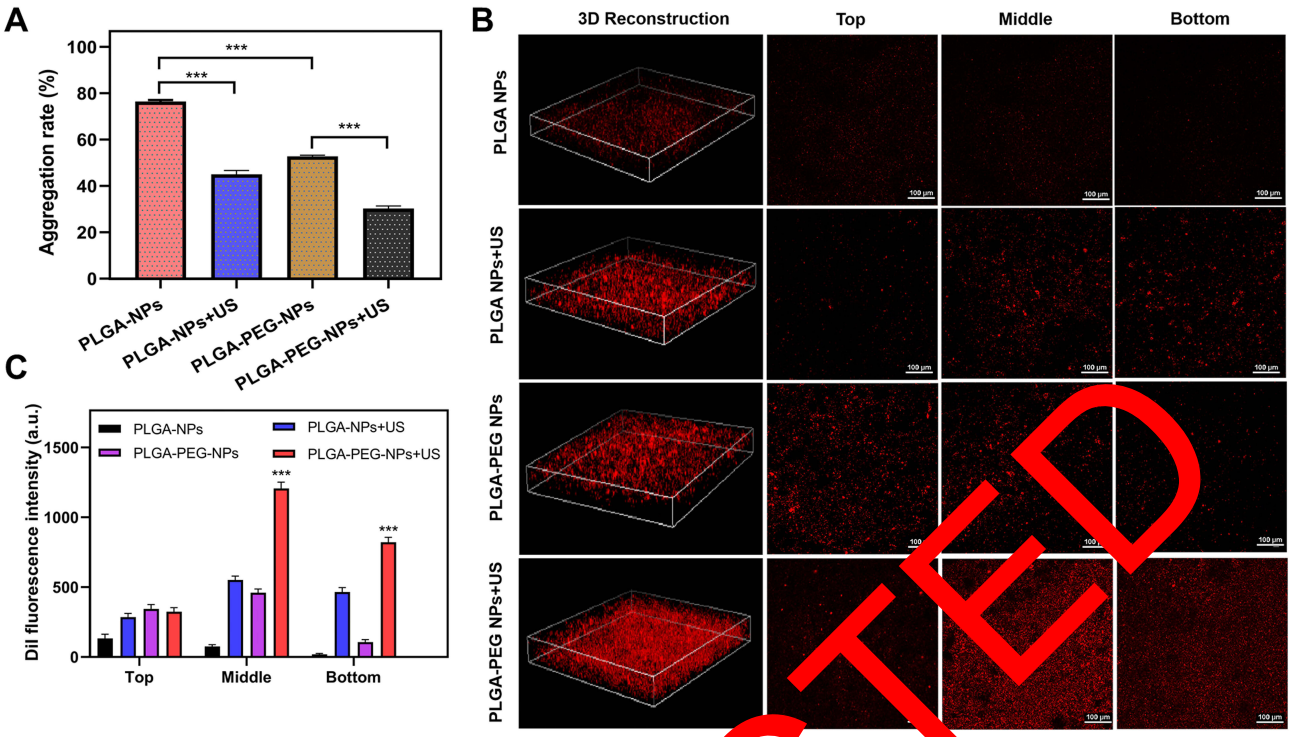

Figure 3 Mucus permeability analysis of PLGA-NPs and PEGylated PLGA-NPs with or without US.
Notes: (**A**) Particle-mucin aggregation rate in mucin solutions. (**B**) The distribution of DiI-labeled red fluorescent nanoparticles in the mucus with or without US irradiation by CLSM observation (scale bar = 100 μm). (**C**) The average fluorescence intensity of DiI in the top, middle, and bottom layers of mucus was calculated by five randomly selected view fields. ***$P < 0.001$.

the receptor chamber was quantitatively calculated within 24 h (Figure 4C). Consistently, the permeation rate of PLGA-PEG NPs+US group was the highest at 67.68% after 24 h incubation, which was 1.78- and 2.88-fold higher than that of PLGA-PEG NPs group alone and non-PEGylated NPs. These data suggest that US-mediated PEGylated NPs possess a superior ability to penetrate the double barrier of mucus and biofilm for mucosa-associated *Candida* infection treatment. This mechanism may be related to the transient cavitation-related generation of high liquid shear forces and acoustic streaming that occurs as a consequence of the US-induced collapse of nanobubbles. Due to their ability to generate a nano-scale mechanical response in a millimeter-scale US field, the bio-effects of US exposure are significantly focused and magnified by the presence of nanobubbles.[29,30]

US Promoted Cellular Uptake of Nanoparticles Under Mucus Barrier

The inefficient diffusion of nanoparticles in mucus will reduce their accumulation near epithelial cells, which will not be conducive to the complete elimination of pathogenic *Candida* invading within the upper cortex, thus easily inducing infection recurrence.[31] Thus, the dynamic VK2/E6E7 cells uptake profiles of various nanoparticles were investigated under the condition of CVM as shown in Figure 5. CLSM observations revealed that the PLGA-PEG NPs+US group exhibited the most obvious and rapid cellular internalization among the four groups. However, individual nanoparticles, either PLGA NPs or PLGA-PEG NPs, could not automatically cross the mucus barrier and be taken up by cells even after 24 hr (Figure 5A). The cellular uptake rate was quantitatively analyzed using flow cytometry at different time points (Figure 5B). Specifically, 22.25% DiI-positive fluorescent cells were detected during the first 2 hr, reaching 75.09% at 24 hr in PLGA-PEG NPs+US group. A higher number of positive cells were detected in the PLGA NPs+US group (57.68%) then that in the PLGA NPs group (15.31%) or PLGA-PEG NPs group (32.57%) at 24 hr. Consistently. The quantitative fluorescence intensity of DiI in the reaction system was also the highest in the PLGA-PEG NPs+US group at all time points (Figure 5C). These data suggest that US could promote the cellular uptake of nanoparticles under mucus conditions, which is conducive to the removal of cell-related biofilms in later studies.

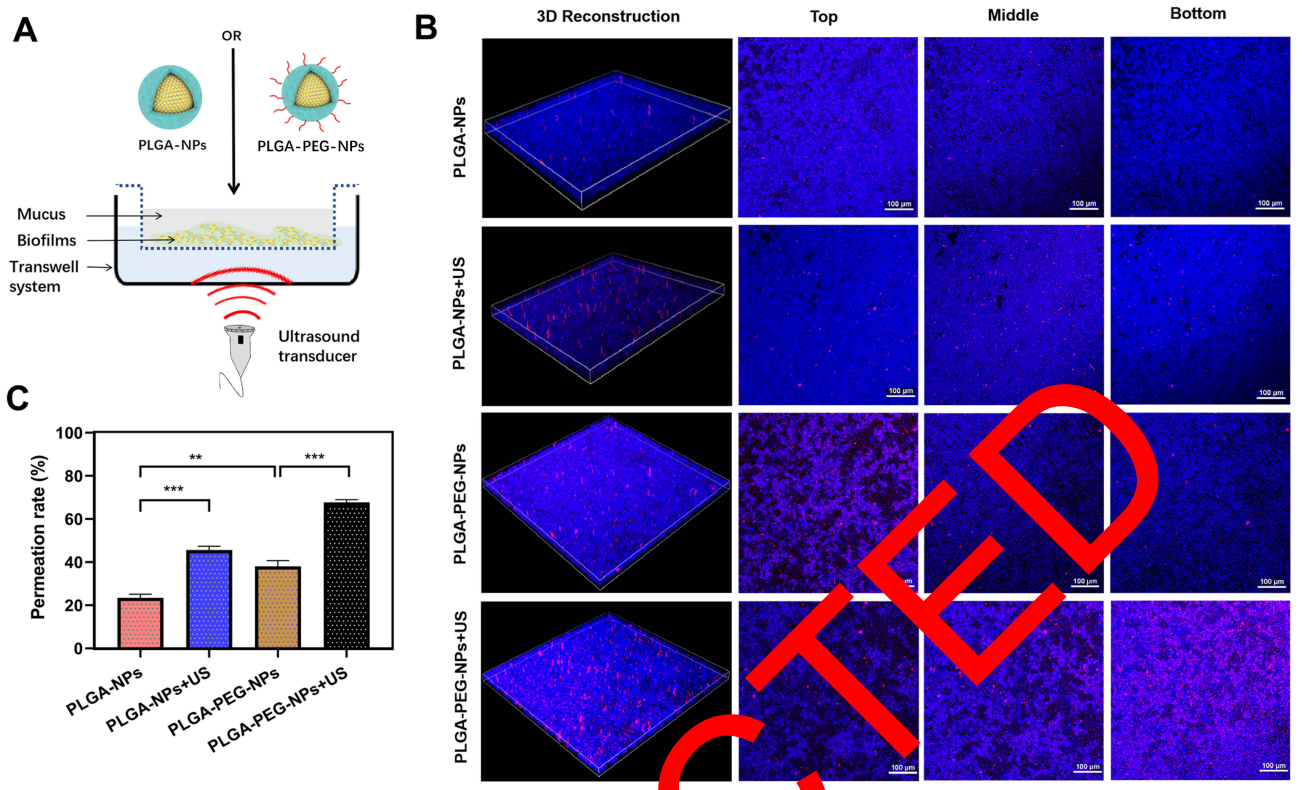

Figure 4 Mucus barrier biofilm penetration assay.
Notes: (**A**) Schematic illustration of the penetration study of US-mediated nanoparticles through a double barrier of mucus and biofilm. (**B**) The penetration of DiI-labeled nanoparticles in the biofilm stained with CFW (blue) under US irradiation after 4 h incubation and observation (scale bar = 100 μm). (**C**) The cumulative permeation (%) of DiI-NPs from the apical of donor chamber to the receptor chamber was calculated within 24 h. $^{**}P < 0.01$, $^{***}P < 0.001$.

Anti-Biofilm Activity of US-Mediated AmB-NPs in the Mucus Barrier

Since the biofilm and mucus layer are both major barriers for the treatment of mucosa-associated *C. albicans* infections, we constructed an in vitro model in which these two important aspects were considered, as shown in Figure 6A. CV staining was first applied to determine the biofilm biomass. Despite the mucus barrier, US+AmB-NPs group still exhibited the strongest anti-biofilm activity, and biofilm biomass was significantly decreased to 48% compared to the control ($P < 0.001$) and the AmB-NPs group ($P < 0.01$), but biofilm biomass was only slightly reduced by AmB or AmB-NPs treatment at low drug concentrations (4 μg/mL) and was not significantly reduced treated with US alone (Figure 6B). The ability of US to eradicate AmB-NPs in biofilms under the mucus barrier was further evaluated by observing the viability of cells in the biofilm and the biofilm architecture using CLSM (Figure 6C). The 3D reconstructed images confirmed that the biofilm in the control group was composed of a large number of live cells and presented dense green fluorescence with many clusters. However, the US+AmB-NPs group displayed the greatest eradicating effect with full destruction of the biofilm architecture and almost all fungi emitting red fluorescence, and the quantitative analysis of the fluorescence intensity of green (live cells)/red (dead cells) also supported the findings of CV assays and CLSM observations (Figure 6D). The morphological characteristics and mycothallus ultrastructural damage to the biofilms following different treatments were further assessed using SEM (Figure 6E). A complete, dense, and thick biofilm structure with wrapped EPS matrix was observed in the control group. The dense biofilm structure is dispersed after ultrasonic irradiation. Treatment with AmB and AmB-NPs alone resulted in minor disruption of the biofilm structure, with a slight reduction in the EPS matrix. In contrast, single yeast colonies within the biofilm became swollen, broken, and inactivated (black arrow), with mycelium fracture and deformity (red arrow) in the US+AmB-NPs group, which further indicated the excellent anti-biofilm activity of US-mediated AmB-NPs treatment even at lower drug concentrations.

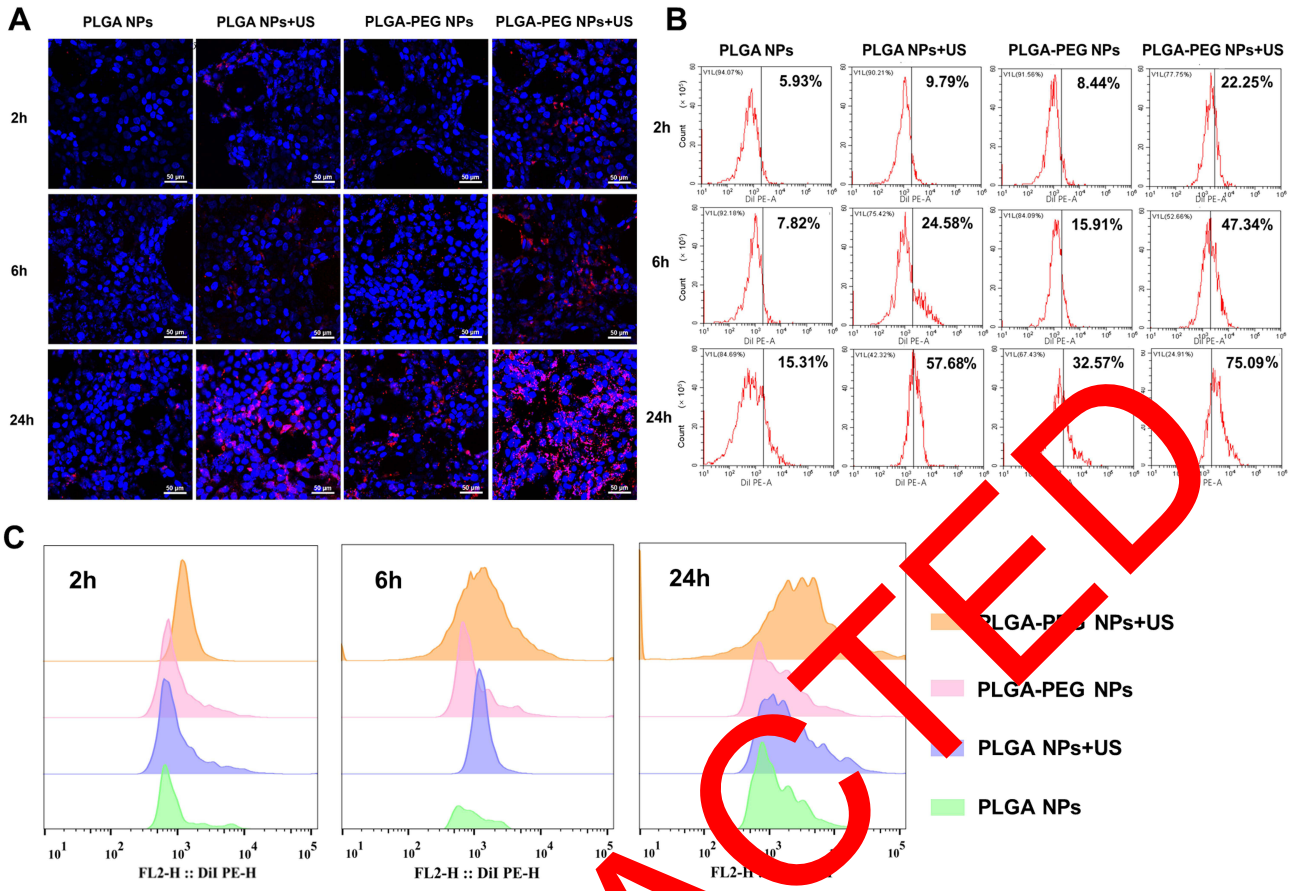

Figure 5 In vitro cellular uptake assay.
Notes: (**A**) CLSM observations of the cellular uptake profiles of VK2/E6E7 cells incubated with DiI-NPs for 2, 6, and 24 h in the presence of the mucus barrier (scale bar = 50 μm). (**B**) Flow cytometric analysis of cellular uptake of nanoparticles under mucus barrier at different times. (**C**) The quantitative fluorescence intensity of DiI in different groups after 2, 6, and 24 h incubation.

Degradation of EPS Relieved Biofilm Hypoxia

C. albicans biofilms are composed of adherent cells and hyphae covered by EPS. The EPS matrix of biofilms mainly consists of polysaccharides and proteins and forms a scaffold for the 3D architecture of the biofilm, which acts as a physical barrier that not only prevents the penetration of antimicrobials but also creates unique conditions in the biofilm hypoxic microenvironment.[4,32] To further explore the anti-biofilm effect of US-mediated AmB-NPs on EPS matrix degradation, the EPS matrix of the biofilm was visually observed by FITC-ConA staining, which specifically binds to the D-(+)-glucose and D-(+)-mannose groups of polysaccharides. In the control group, *C. albicans* formed biofilms characterized by large aggregates and an abundant matrix of EPS, but the EPS matrix structure became looser after US irradiation, and the matrix was significantly reduced after US combined with drug treatment, especially when treated with US+AmB-NPs, which also displayed the strongest elimination of EPS, with a small amount of scattered green fluorescence (Figure 7A). The elimination of EPS was further probed by quantitative determination of extracellular polysaccharides and proteins (Figure 7B and C). Similarly, the contents of polysaccharide and protein in EPS matrix of biofilm were significantly reduced by 80.2% and 57.2%, respectively, after US+AmB-NPs treatment compared with the control group (both $P < 0.01$), with the lowest content among the groups.

After identifying the EPS degradation properties of US-mediated AmB-NPs, their ability to relieve hypoxia in the biofilm was further evaluated. During biofilm formation, 3D reconstruction of the biofilm showed that hypoxia inside the biofilm gradually increased from 12 to 72 h, showing an obvious time-dependent characteristic (Figure S1). However, hypoxia in the *C. albicans* biofilms was significantly relieved after US-mediated AmB-NPs treatment, with the lowest red fluorescence signal expression compared with the other treatment groups (Figure 7D). Specifically, the red hypoxic area was reduced by nearly 80% compared with the control group (Figure 7E), indicating US-mediated AmB-NPs treatment can effectively improve the degree of hypoxia in biofilms in vitro. Hypoxia is a typical characteristic of almost all

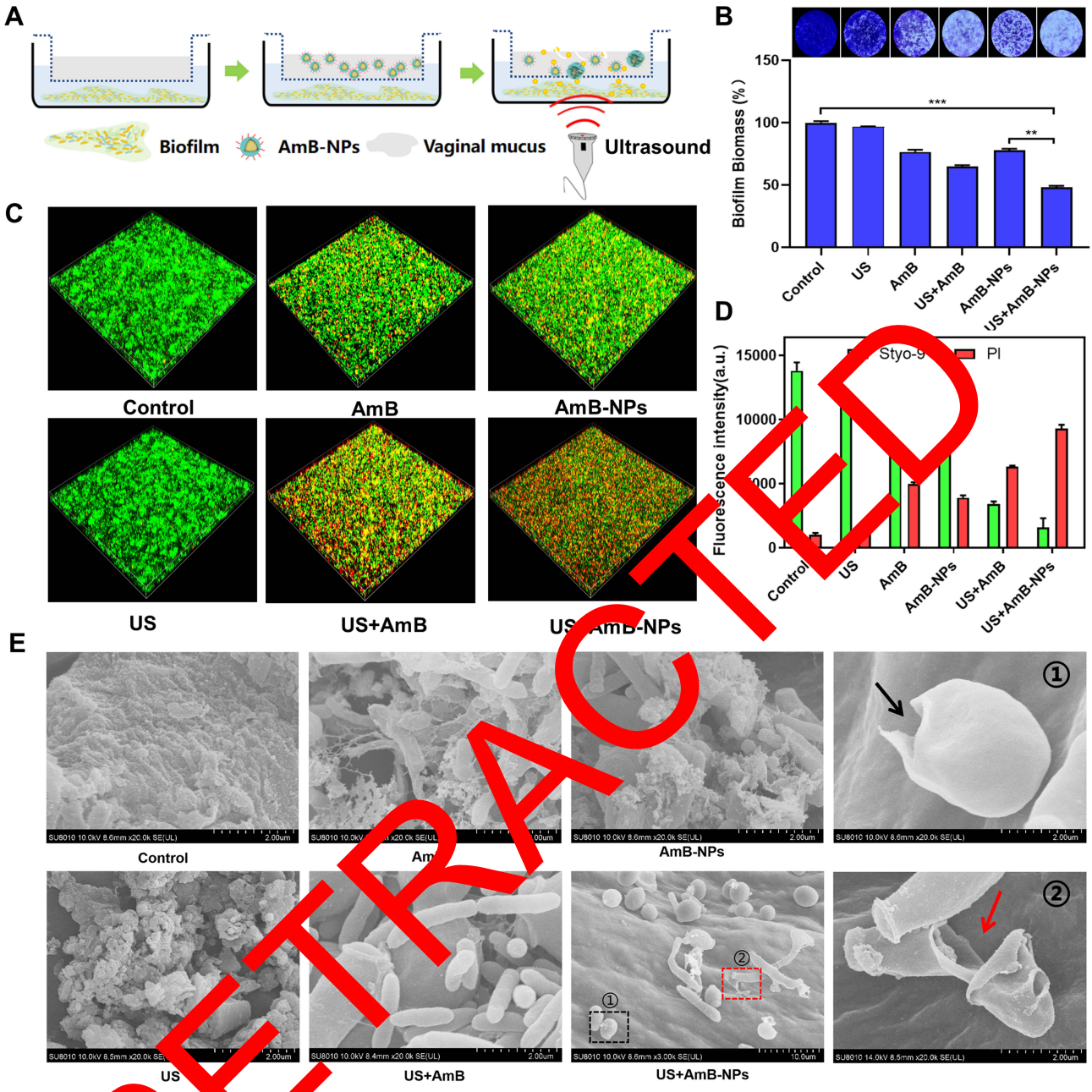

Figure 6 (**A**) Schematic illustration of biofilm effect of US-mediated AmB-NPs in the mucus barrier using a transwell system. (**B**) Analysis of biofilms biomass by the crystal violet staining after treatment with different groups. (**C**) Observation of the viability cells of biofilm and biofilm architecture after SYTO 9 (Live) / PI (dead) staining using CLSM 3D reconstructions. (**D**) The quantitative fluorescence intensity of SYTO 9 and PI in the different group to analyze the ratio of live and dead fungi. (**E**) SEM observation of biofilm elimination and mycothallus ultrastructure damage in different groups.

Notes: $^{**}P < 0.01$, $^{***}P < 0.001$. (**E**) Scale bar = 2 μm, the black arrow indicates inactivation and rupture of *C. albicans* yeast and the red arrow indicates mycelium fracture and deformity in the US+AmB-NPs group.

biofilms and is an important reason for the antibiotic resistance of biofilm-encased bacteria. In many previous studies, oxygen was transmitted by nanocarriers or produced in situ through the catalytic function of enzymes.[33,34] In this study, US-mediated AmB-NPs therapy could also affect the hypoxic microenvironment of biofilms, which might be achieved by destroying the structure of biofilms and excellent osmotic promotion.

US-Mediated AmB-NPs Induces Biofilm Intracellular ROS Generation

SDT is a novel antibacterial strategy that can efficiently eliminate bacteria by generating ROS under US stimulation, among which, ROS generation is a critical factor in conventional SDT-induced cell apoptosis.[35] Therefore, an

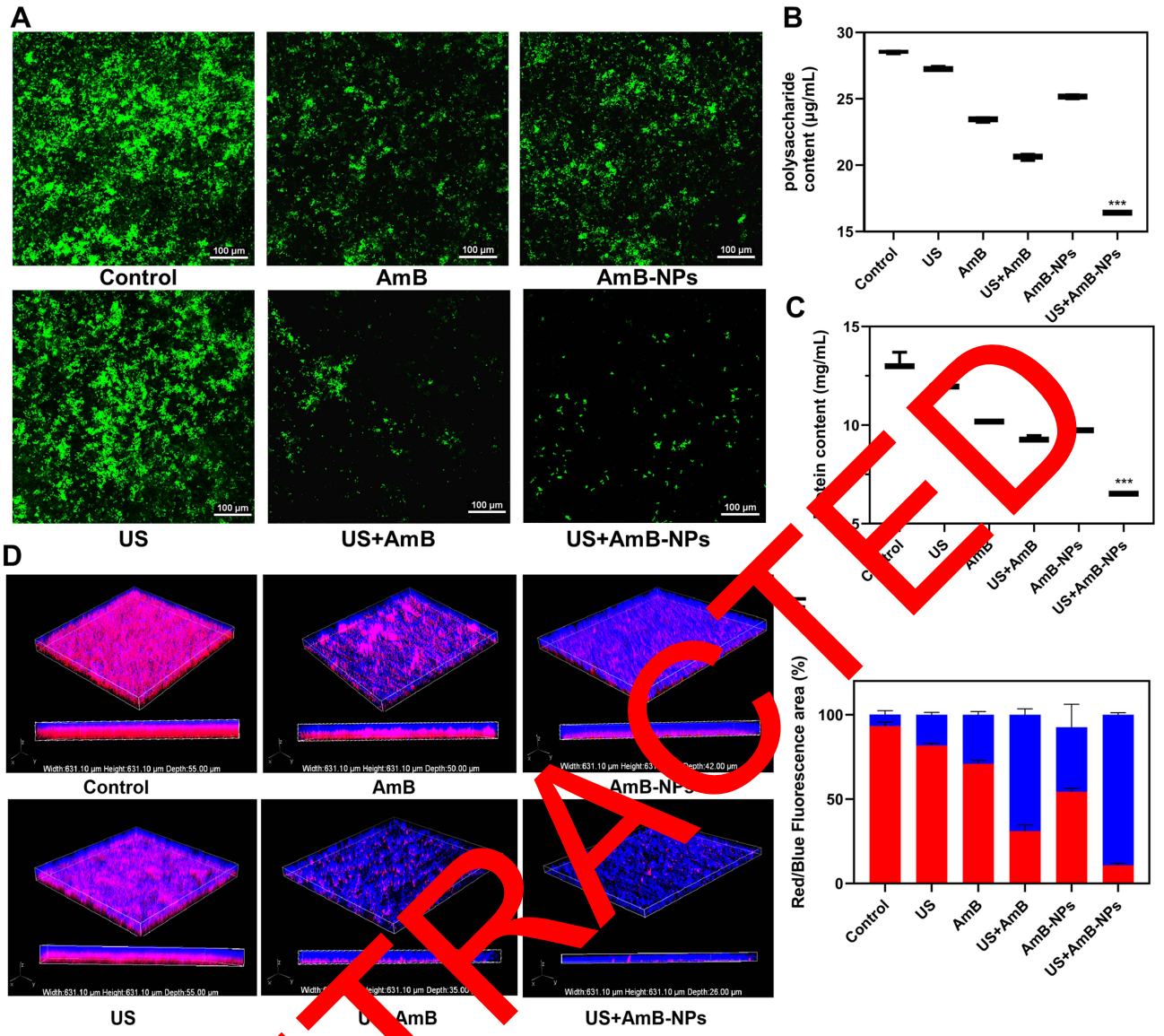

Figure 7 (**A**) The anti-biofilm effect of US-mediated AmB-NPs on EPS matrix elimination analysis. The quantitative determination of extracellular polysaccharide (**B**) and protein (**C**) in EPS using phenol-sulfuric acid method and BCA protein assay kits, respectively. (**D**) Analysis of hypoxia changes in biofilm using CLSM 3D reconstruction images. (**E**) The quantitative calculation of red/blue fluorescence area to reflect the hypoxic range after treatment in different groups.
Notes: (**A**) EPS in biofilm was stained with FITC-ConA (green) and observed using CLSM (scale bar = 100 μm). (**B** and **C**) ***$P < 0.001$ vs Control. (**D**) Hypoxia areas were examined with a Image-iT™ hypoxy probe (red) and the *C. albicans* biofilms profile were labeled with CFW (blue).

intracellular ROS assay based on DCFH-DA was used to further evaluate the feasibility of SDT anti-biofilm therapy-based US-mediated AmB-NPs. As shown in Figure 8A, more ROS, indicated by green fluorescence, were observed in the US+AmB-NPs group than in the other groups. This may be related to the fact that nanoparticles volumetric oscillations facilitate cavitation-related phenomena and induce stronger sonochemical reactions to enhance the efficiency of ROS generation.[36] Then, to identify which ROS species are involved in US-mediated AmB-NPs SDT anti-biofilm, three representative types of ROS were measured using DHE, HPF, and SOSG to detect O_2^-, ·OH, and $^1O_2$ generation, respectively. Quantitative analysis of the FI of DHE and HPF confirmed that O_2^-, ·OH, and $^1O_2$ generation increased in the AmB-NPs+US treatment, but ·OH and $^1O_2$ had a higher FI (Figure 8B–D). This is consistent with previous reports that ·OH was the main ROS species after US exposure, which may be due to cavitation bubbles induced by US irradiation producing high local temperatures upon collapse, thus generating ·OH by water pyrolysis.[35,37] $^1O_2$ is a type II ROS mediated by sonoluminescence and induces photooxidation of cellular components, thereby causing cell death.

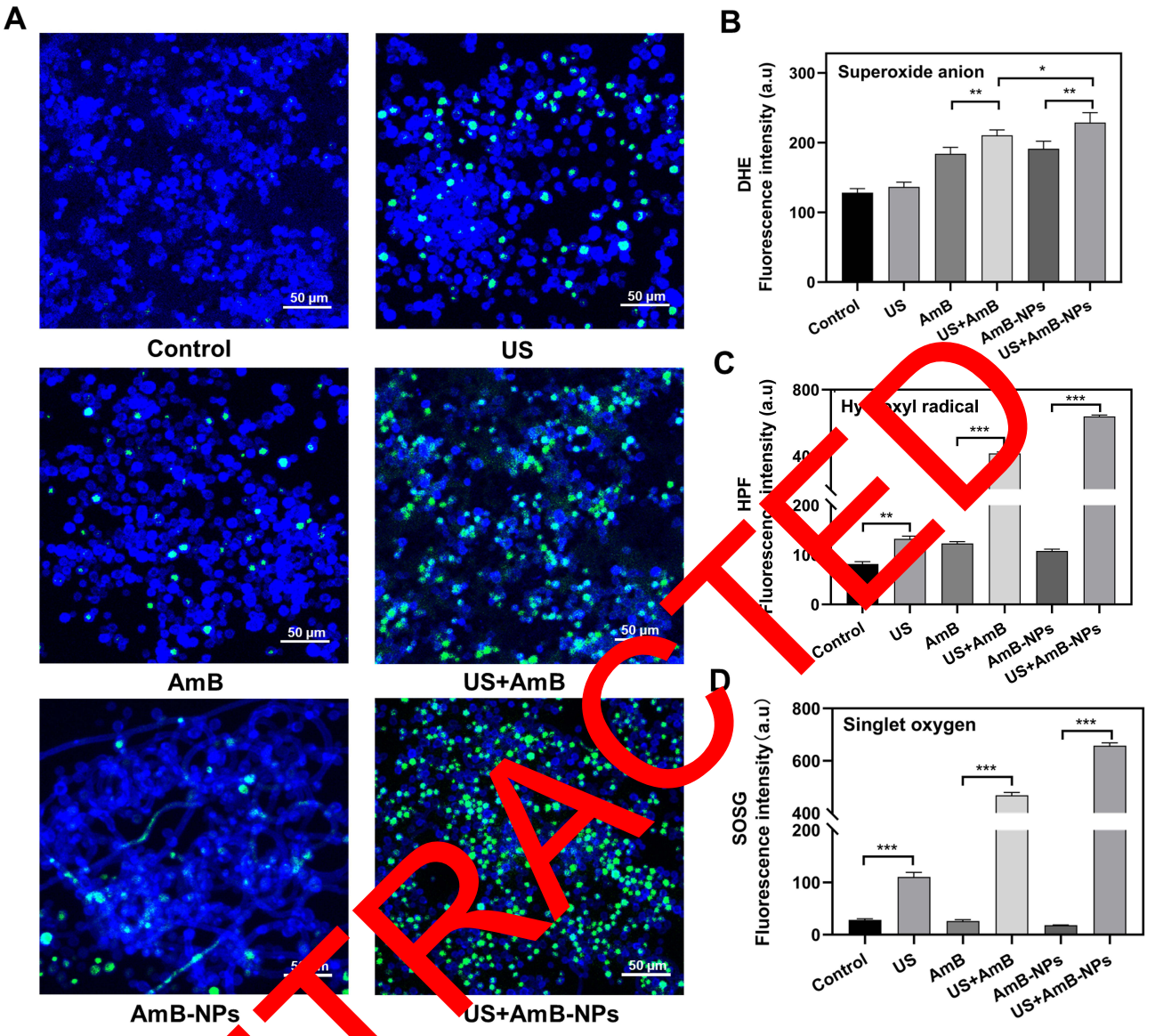

Figure 8 Detection of ROS and subspecies generation.
Notes: (**A**) The production of intracellular ROS (green) within the biofilm (blue) was observed by CLSM following treatment with different modalities (scale bar = 50 μm). (**B–D**) Detection of ROS subspecies superoxide anion (O_2^-), hydroxyl radical (·OH), and singlet oxygen ($^1O_2$) after the biofilm treatment with different methods and incubated for another 2 h. *P < 0.05, **P < 0.01, ***P < 0.001.

Usually, moderate ROS generation is necessary to preserve cells. However, excess ROS accumulation inside the cell results in oxidative damage to DNA, proteins, membranes, and organelles, resulting in cell death, which is also an important synergistic anti-biofilm mechanism in this study.[38]

Effect of US-Mediated AmB-NPs on Epithelium-Associated Biotic Biofilms

Epithelium-associated biotic biofilms are grown on active mucosal surfaces where *C. albicans* interacts with epithelial cells, which may differ from abiotic biofilms in many different ways, including their functioning fixedness and susceptibility to conventional antifungals.[39] After confirming the excellent ability of mucus penetration and biofilm removal on abiotic surfaces of US-mediated AmB-NPs effect, we further investigated the sonodynamic penetrated therapy of US-mediated AmB-NPs on epithelial cell-associated candida infections and the schematic diagram as shown in Figure 9A. The dynamic process of *C. albicans* invading epithelial cells to form biofilms showed that a large number of *C. albicans* adhered to the VECs within 2 h, mycelia formed and infiltrated the cells at 6 h, and biofilm formation was

visible after 24 h of co-incubation (Figure 9B). The biofilm formation time was shorter than that of the culture on microplates, which also indicated that the formation of epithelium-associated biotic biofilms was different from that on abiotic surfaces. Then, the VECs-*C. albicans* co-culture system was pretreated with US and AmB-NPs separately or jointly and observed in the early phase after 6 h of incubation. The combined effect of US and AmB-NPs exhibited the strongest inhibitory effects on *C. albicans* adhesion, with very few *C. albicans* around cells, and no obvious intracellular infiltration was observed (Figure 9C). Moreover, the quantitative FI of SYTO 9-labeled *C. albicans* in the reaction system was also the lowest in the US+AmB-NPs group at 2228.7±47.5, which was more than a fivefold reduction compared to the control group (12,454.5±28.8) (Figure 9E). Generally, early adherence and mycelial phase transition to infiltrate epithelial cells are two key steps in biofilm formation in mucosal-associated *Candida* infections in vivo.[3] This result further confirmed the efficacy of US-mediated AmB-NPs in inhibiting *C. albicans* adhesion and infiltration and preventing biofilm re-formation.

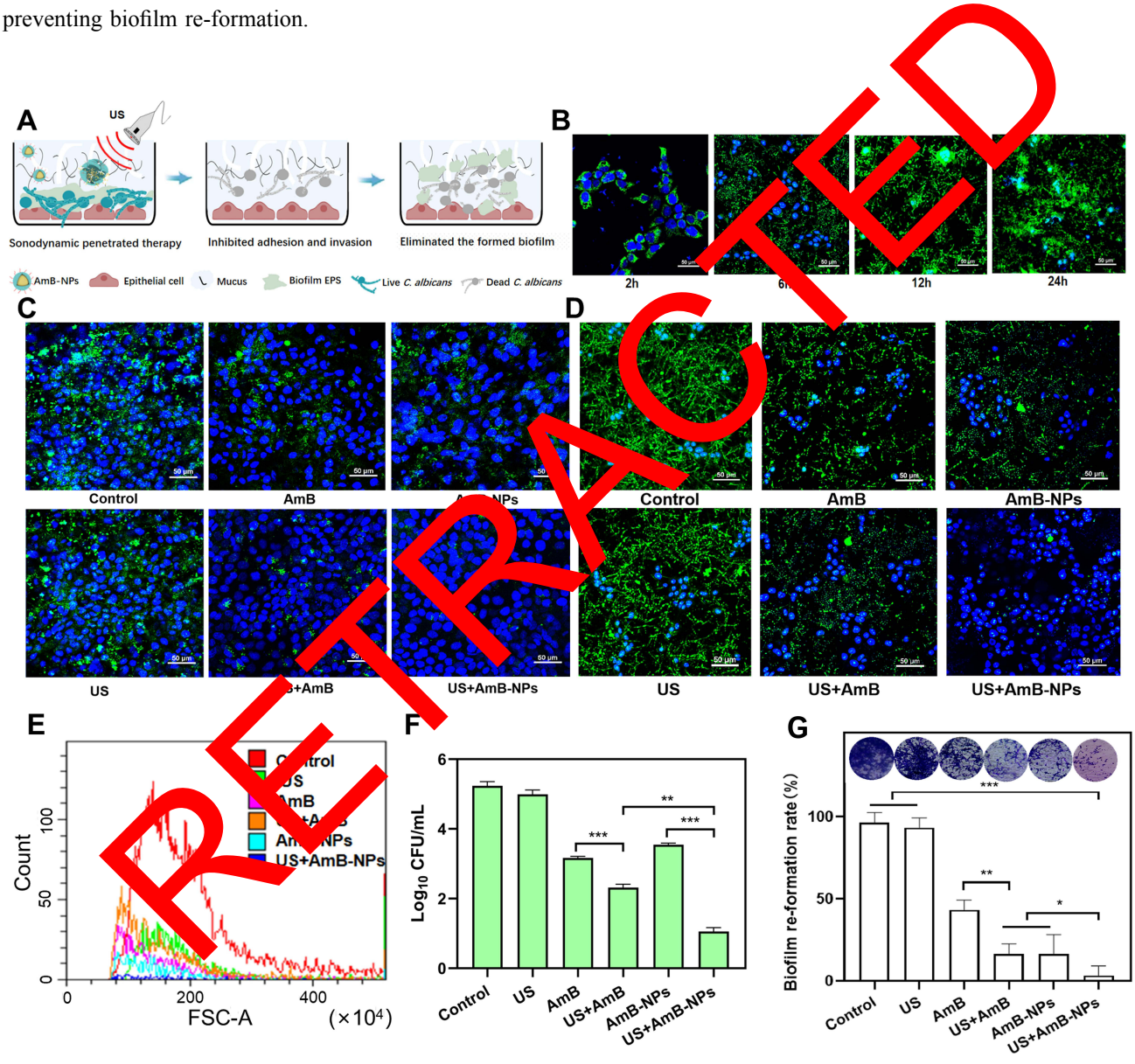

Figure 9 Human vaginal epithelial cell related anti-biofilm assay.

Notes: (**A**) Schematic illustration of anti-biofilm effect of US-mediated AmB-NPs in a co-culture model of VK2/E6E7 epithelial cell and *C. albicans* in the presence of mucus. (**B**) The process of *C. albicans* (FITC-labeled, green) adhesion, infiltration, and biofilm formation on the cell (DAPI-labeled, blue) surface from 2 to 24 h co-culture under CLSM observation (scale bar = 50 μm). (**C**) Inhibition of early adhesion and infiltration of *C. albicans* to VECs after US-mediated AmB-NPs treatment (scale bar = 50 μm). (**D**) Elimination effect of biofilms formed on VECs surfaces was observed by CLSM following different treatment (scale bar = 50 μm). (**E**) The adhesion rate of *C. albicans* to cells was quantitatively detected by flow cytometry. (**F**) CFU analysis of *C. albicans* cultures from biofilm after 24 h of treatment by different modalities. (**G**) Biofilm re-formation rate was analyzed using crystal violet staining for biofilm formation observation. **P* < 0.05, ***P* < 0.01, ****P* < 0.001.

The elimination effect of US-mediated AmB-NPs on mature *C. albicans* biofilms formed on VECs surfaces in the presence of mucus was further verified. As indicated in Figure 9D, the *C. albicans* biofilm in the control group showed a classic compact biofilm structure with both yeast cells and hyphal elements distributed on the cell surface and apparently internalized by epithelial cells. However, US-mediated AmB-NPs almost completely removed the biofilm structure on the cell surface, with the lowest fluorescence signal compared to the other treatment groups. Moreover, AmB-NPs+US group showed the lowest fungi number of (1.057±0.11) Log_{10} CFU/mL and the fungicidal rate was more than 100-folds higher than that of free AmB (Figure 9F). In addition, US combined AmB-NPs effect could almost completely inhibit biofilm re-formation with inhibition rates up to of 97.3% (Figure 9G), also demonstrating the superior anti-biofilm efficacy and inhibition of biofilm regeneration effect of US-mediated AmB-NPs on epithelium-associated biotic biofilms.

Effects on Ultrastructural and Immune Function of Infected VECs

For further insight into the interactions of *C. albicans* with VECs, the internal ultrastructural changes of VECs and the adherence and invasion of *Candida* in different groups were observed using TEM. As shown in Figure 10A, in the control group, large numbers of *C. albicans* yeast colonies and mycelia were scattered and distributed around the infected cells, which were severely damaged with necrosis, disintegration, and scattered cell fragments (yellow arrow). Simultaneously, the plasma membrane of the cell ruptured and cell components spilled in the US group, and appearance of pseudohyphae structures inserted into the cell in a process (white arrow) that may be one of the mechanisms used for epithelial cell invasion.[40] After AmB or AmB-NPs treatment, the ultrastructure of cell damage was slightly improved, but the mitochondria were still swollen obviously (black arrow), and autophagosomes were formed (red arrow). However, the initially observed invasive blastoconidia and hyphae were significantly reduced or completely absent after 24 h of the US-mediated AmB-NPs treatment. More importantly, the cell morphology and vitality were significantly improved, with a normal shape, relatively intact and smooth cell membrane, normal mitochondrial structure, and few autophagosome reservations. VECs autophagy plays an indispensable role in the host response to vaginal infection by *C. albicans*, particularly in the activation and recruitment of adaptive immune responses to eliminate pathogenic bacteria.[41]

Since mucosal epithelial cells produce a variety of cytokines and chemokines in response to microorganisms and *C. albicans* is closely associated with mucosal epithelial cells as a commensal, we further analyzed the levels of IL-2, IL-4, IL-10, and IL-17 in the culture supernatants of VECs after treatment. Cytokines IL-2, IL-17, IL-4, and IL-10 were all upregulated in the culture supernatants of VECs after infection compared with normal cells (Figure S2). However, 24 h post-treatment, the levels of IL-2 and IL-17 increased significantly, but the levels of IL-4 and IL-10 in the US+AmB-NPs -treated culture supernatants were lower than those in the control groups (Figure 10B). Epithelial cells of host mucosal surfaces represent the first line of defence against *Candida* infection and the cytokines produced by epithelial cells are one of important defense mechanisms involved in epithelial cell responses to *Candida* invasion.[42] IL-2 and IL-4 are the classical representatives of Th1 and Th2 cytokines, respectively. Th1-type cytokines play a strong role in mediating immunity against *Candida* to be beneficial for pathogen or cancer elimination, while Th2 responses correlate with disease exacerbation inflammation progression.[43] Our results revealed that the increased expression of IL-2 and the decreased expression of IL-4 in the US+AmB-NPs group, which indicated that US-mediated AmB-NPs treatment can indirectly up-regulate the vaginal local cellular immunity under the infective status to promote the host defense against invading pathogenic microorganisms.

Increase in Phagocytosis and Regulation of Macrophage Polarization

In addition to the local antifungal immunity of epithelial cells, macrophage is also one of the most critical regulator in multiple biological processes. In response to pathophysiologic conditions such as mucosal candidiasis, phagocytosis by macrophages and their macrophage polarization state are key factors in the host's resistance to pathogens and anti-bacterial action, which determine the control and outcome of infection.[44] We coincubated macrophages with *C. albicans* for a phagocytosis assay and found that US stimulation could significantly enhance the phagocytosis ability of macrophages. Quantitative analysis of phagocytosis by flow cytometry showed that the percentage of phagocytosis was significantly higher in the US groups, and the phagocytosis rate was up to 68% after 300s irradiation, 3-folds higher

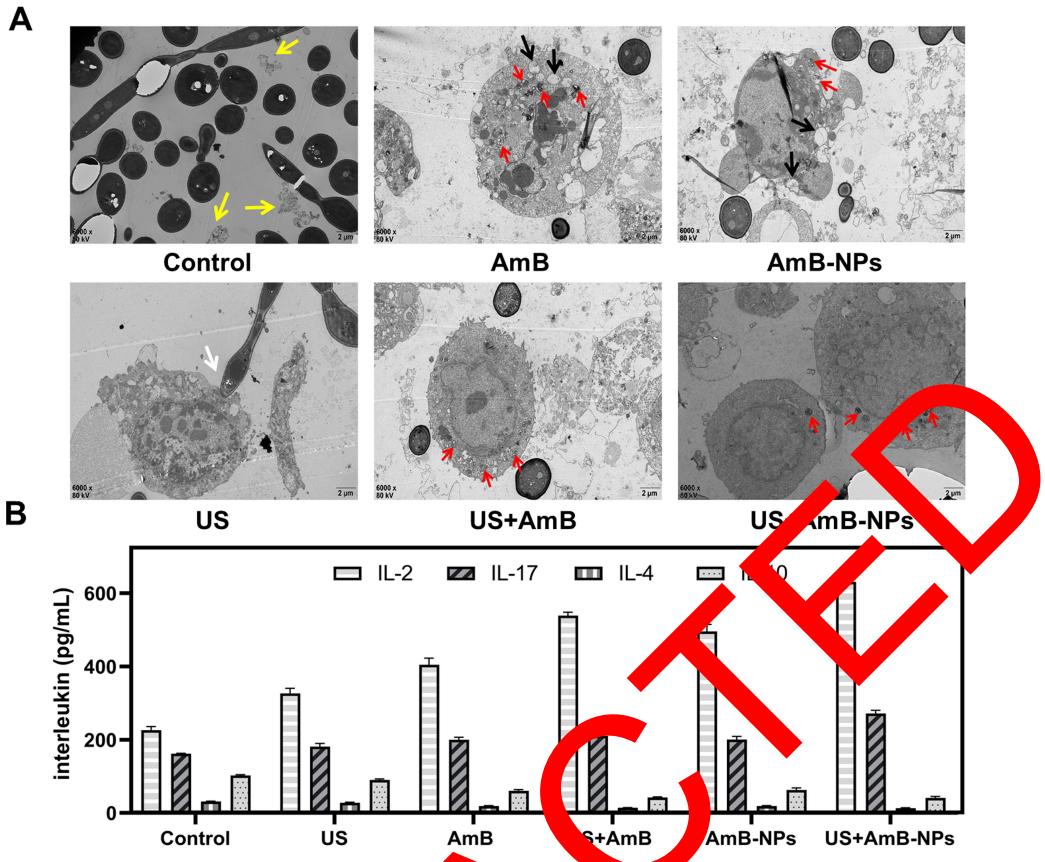

Figure 10 (**A**) TEM observation the internal ultrastructural changes of the VE[illegible] and [illegible]dherence and invasive of *Candida* in different group. (**B**) ELISA analysis of the levels of IL-2, IL-17, IL-4 and IL-10 cytokines in the culture supernatants of VECs [illegible] differe[illegible]ent groups.
Notes: (**A**) The yellow arrow shows cell fragmentation, white arrow shows the [illegible]eu[illegible]yphae structures inserted into the cell, black arrow shows the mitochondria swollen, and red arrow shows autophagosomes formed (scale bar[illegible]

than that in the control group (Figu[illegible]11B). P[illegible]ocytosis of pathogenic bacteria and foreign bodies by macrophages is the basis of wound debridement [illegible]u[illegible]g the infla[illegible]matory period, and low-intensity US can enhance phagocytosis of macrophages by promoting a[illegible]tin polyme[illegible]zation and activating extracellular regulatory protein kinase and p38 mitogen-activated protein kinase s[illegible]naling pathways.[illegible]

SDT can generate [illegible]OS to f[illegible]m an oxidative stress microenvironment that induces not only tumor cell apoptosis but also M1-type macropha[illegible]o[illegible]rization [illegible] antitumor applications.[46] To further investigate the immunoregulatory effects of US-mediated A[illegible]B-[illegible]Ps trea[illegible]ment [illegible] the inflammatory response of *C. albicans* infection, polarization of macrophages experiment[illegible]as perfo[illegible]med as de[illegible]icted in Figure 11A. *C. albicans* infection promoted M1 polarization of Raw264.7 cells, and higher i[illegible]re[illegible]ent exp[illegible]ssion of CD86 was observed in the US+AmB-NPs group, and the *C. albicans* clearance effect was obvi[illegible]. Simultaneously, the expression of CD86 was also enhanced in the LPS-induced M1 polarization model after US-me[illegible]ted AmB-NP treatment. In contrast, the fluorescence expression of CD206 significantly decreased in the IL-4-induced M2 model in the US+AmB-NPs group (Figure 11C). Moreover, the expression of the M1-type markers IL-1β and TNF-α was significantly increased, whereas that of the M2 markers IL-10 and TGF-β was significantly decreased in the US+AmB-NPs group (Figure 11D). Macrophages can function as different phenotypes, such as M1 and M2 macrophages, M1-type plays a role in presenting antigens, secreting inflammatory factors, phagocytic sterilization, initiating adaptive immune responses, and play a major role in host defense against various microbial pathogens, including fungi.[44,47] Finally, the results demonstrated that US-mediated AmB-NPs could increase the phagocytosis by macrophages and regulate the polarization of macrophages to the M1 phenotype, thus enhancing the efficient elimination of pathogenic fungi through the dual action of bacteriostasis and immune activation.

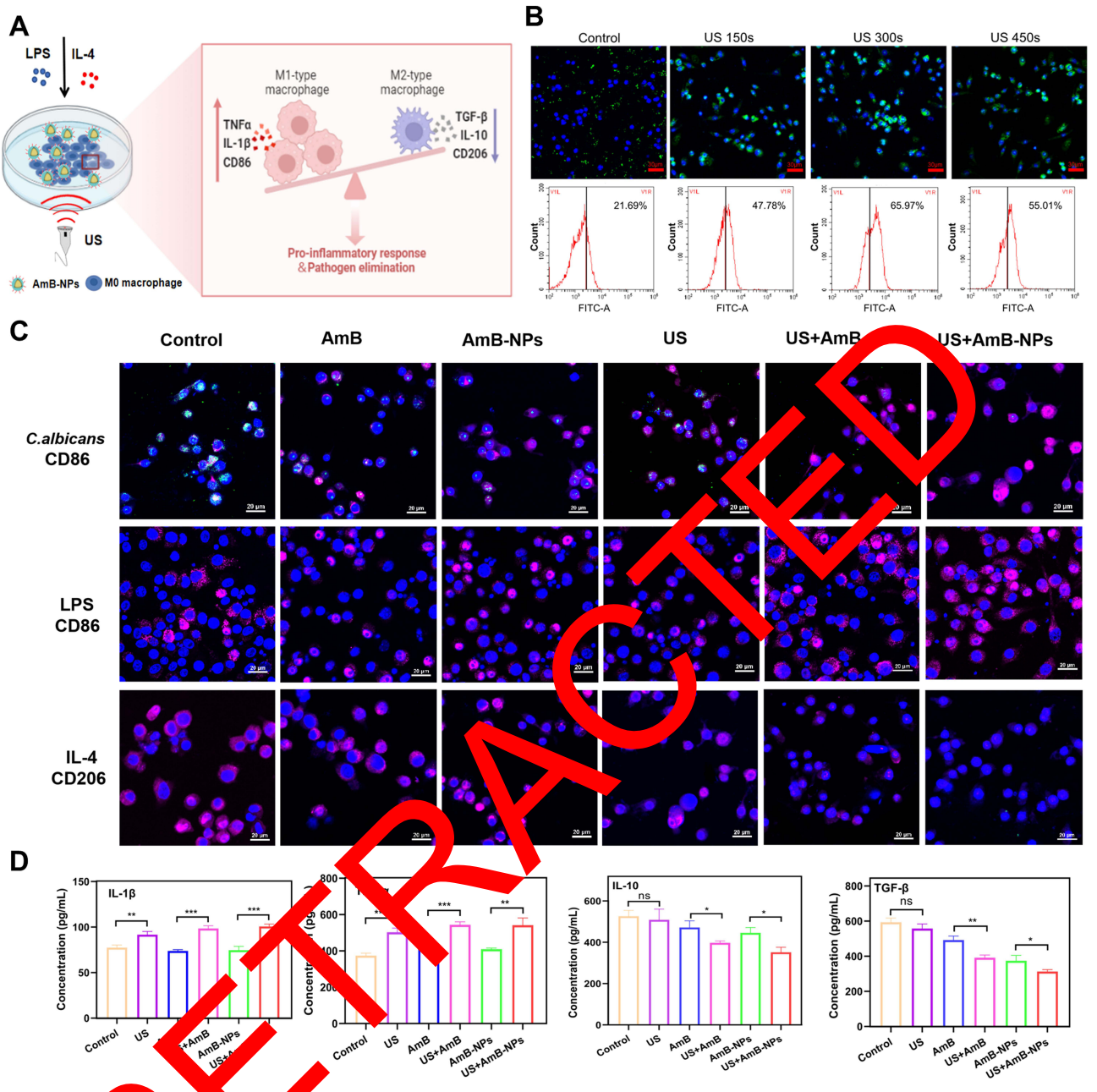

Figure 11 Analysis of macrophage polarized antifungal immune responses induced by US-mediated AmB-NPs treatment.
Notes: (**A**) Schematic diagram of US-mediated AmB-NPs regulating RAW264.7 macrophage polarization between M1 phenotype and M2 phenotype. (**B**) CLSM observation of the phagocytosis by macrophages of FITC-labeled *C. albicans* (green) and flow cytometry analysis of the percentage of phagocytosis after ultrasonic irradiation for different times. (**C**) Immunofluorescence images of macrophage cells by different treatments showing CD86 and CD206 expression (scale bar = 20 μm). RAW264.7 cells were induced to M1 or M2 type macrophages with 1 μg/mL LPS or 50 ng/mL IL-4, respectively. (**D**) ELISA analysis on the expression of M1 type-related markers (IL-1β, TNF-α) and M2 type-related markers (IL-10, TGF-β) in macrophages following treatment with different modalities. "ns" indicates no statistical difference, *$P < 0.05$, **$P < 0.01$, ***$P < 0.001$.

Antifungal Effects of US-Mediated AmB-NPs on Rabbit Vaginal *C. albicans* Biofilms

To further assess its potential as an effective strategy for biofilm-associated mucosal candidiasis, we demonstrated the antifungal effects of US-mediated AmB-NPs on rabbit vaginal *C. albicans* biofilms in vivo and the treatment scheme is shown in Figure 12A. The antifungal efficiency of the different treatment modalities was studied by measuring the number of fungi in the vaginal washes on the third day post-treatment (day 14). The cell viability and colony formation of *C. albicans* were significantly decreased in the US+AmB-NPs group compared to the other treatment groups (Figure 12B), indicating the excellent antifungal efficiency of US-mediated AmB-NPs in vivo. Histochemical analysis

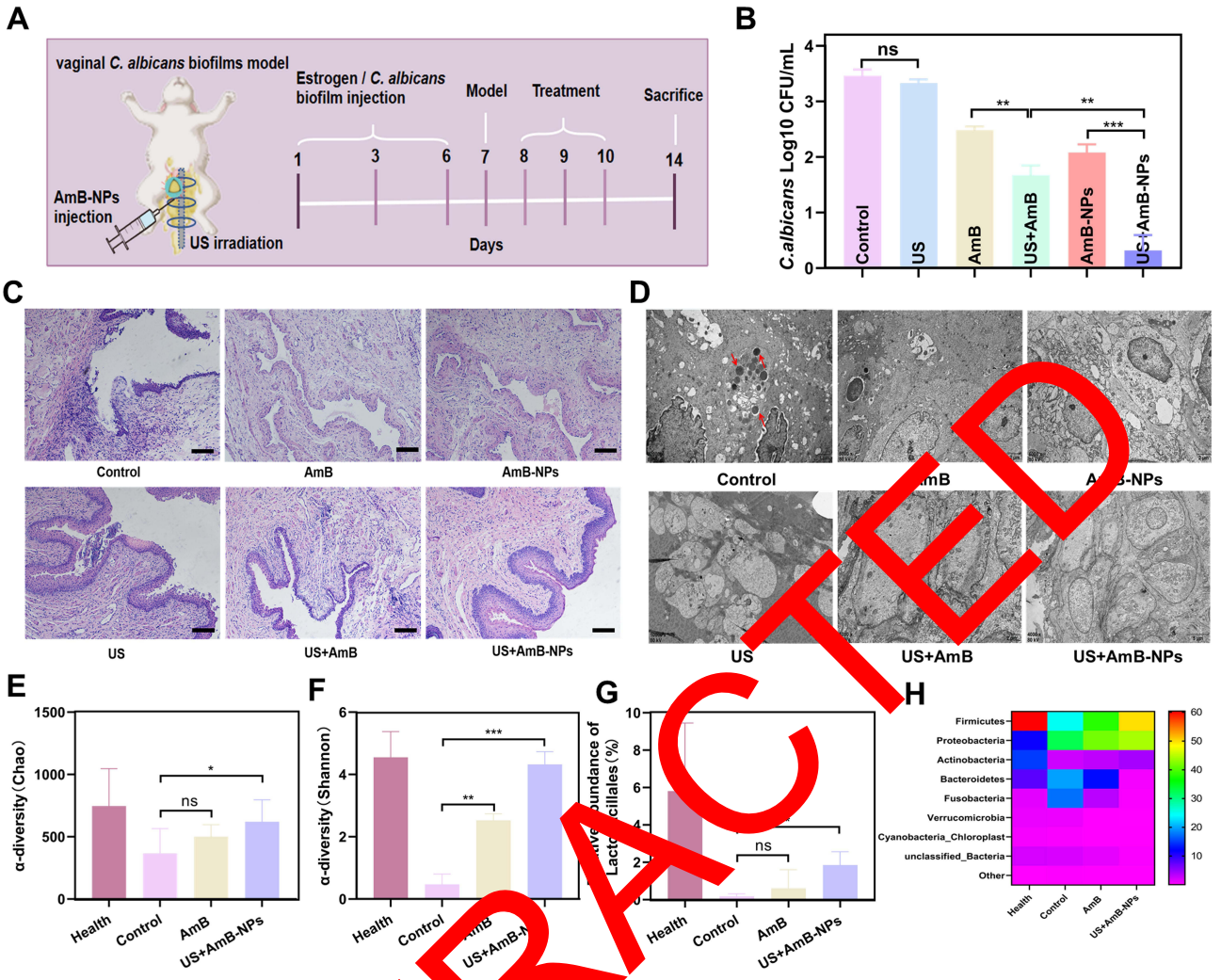

Figure 12 Antifungal effects of US-mediated AmB-N[illegible] on vagina[illegible] *albicans* biofilms in vivo.

Notes: (**A**) Experimental scheme of *C. albicans* v[illegible] biofilms rabbit[illegible]del. (**B**) Count of viable of *C. albicans* in vaginal washes after indicated treatments. (**C**) H&E staining images of the vaginal tissue (scale bar = 50 μm) and (**D**) TEM images for [illegible]aginal epithelium ultrastructure observation in different treatment modalities (scale bar = 2 μm, the red arrows show yeasts and hyphae penetrated supe[illegible]ial layers of the vaginal mucosa and immersed epithelial cell). (**E** and **F**) α-Diversity Chao and Shannon indexes of the vaginal microbiome by 16S rRNA ge[illegible]sequencing. (**G**) [illegible]ative abundance of order-level taxa for *Lactobacillales*. (**H**) Heatmap of the relative abundance of phylum-level taxa for each group. "ns" indicates [illegible]statistical difference, *P [illegible].05, **P < 0.01, ***P < 0.001.

showed that an obvious *C. albicans* biofilm-like structure was formed by mycelium colonies invading the vaginal epithelium and causing serious damage to the vaginal mucosa with massive inflammatory cell infiltration in the control and the US group. Inflammatory infiltration was slightly relieved by treatment with AmB or AmB-NP alone. The invasion of *Candida* mycelium in the vaginal epithelium and submucosal inflammatory cell infiltration were significantly relieved, and the epithelial structure of the vaginal mucosa was roughly restored with stratum corneum formation in the US+AmB-NPs group (Figure 12C). Subsequently, the ultrastructure of the vaginal epithelium was observed using TEM (Figure 12D). Following infection with *C. albicans*, the entire epithelial layer was destroyed and VECs exhibited ultrastructural impairment, including cytoskeleton disintegration, incomplete plasma membrane rupture, nucleolysis, desmosome damage, and increased intercellular space (Figure S3A). In addition, a greater number of yeasts and hyphae penetrated the superficial layers of the vaginal mucosa and immersed epithelial cells (red arrow). However, the ultrastructure of the vaginal epithelium was notably improved after US-mediated AmB-NPs treatment, which showed that stratified epithelial cells were arranged in an orderly manner, and new immature epithelial cells were formed to promote the repair of the vaginal mucosa (Figure S3B). Next, the amelioration of the vaginal microbiome in *C. albicans*-induced vaginitis after US-mediated AmB-NPs treatment was investigated using 16S rRNA gene sequencing. Analysis of

vaginal wash samples revealed that the Chao and Shannon entropy indices of α-diversity were significantly increased in the US+AmB-NPs group, indicating that bacterial diversity markedly improved after US treatment (Figure 12E and F). Furthermore, the relative abundance of *Lactobacillus* significantly increased (Figure 12G), which is thought to reinforce the defense against invasion and colonization by pathogenic microorganisms and promote the maintenance of vaginal homeostasis. Further analysis at the phylum level revealed that US treatment markedly increased the relative abundance of *Firmicutes*, reshaping the healthy vaginal microbiome (Figure 12H). On the basis of effective antifungal results obtained in the previous study of US-mediated AmB-NPs therapy for VVC infection,[20] these part results further confirmed that US-mediated AmB-NPs treatment exhibits excellent therapeutic efficacy against *C. albicans* vaginal biofilms in vivo, promotes the recovery of damaged mucosal epithelial ultrastructure, and contributes to the reshaping of a healthier vaginal microbiome.

Conclusion

Biofilms and mucus layers are both major barriers in the treatment of mucosa-associated *C. albicans* infections. Herein, a novel anti-biofilm strategy of mp-SDT based on US-mediated AmB-NPs was systematically investigated to overcome both biofilm and mucus layer obstruction and effectively eradicate *C. albicans* biofilm under the synergistic enhancement effect of SDT and chemotherapy with antibiotic AmB. This mp-SDT regimen was verified to easily penetrate mucus and disperse the dense biofilm structure, simultaneously activating AmB to produce high concentrations of ROS in the biofilm and exhibiting excellent anti-biofilm effects in vitro and in vivo. Moreover, mp-SDT strategy promoted ultrastructural repair and local immune defense enhancement of epithelial cells, regulated the polarization of macrophages to the M1 phenotype to enhance macrophage-associated antifungal immune responses, and contributed to reshaping a healthier vaginal microbiome for *Candida* vaginitis therapy. Therefore, we implemented a promising strategy to effectively eradicate *C. albicans* hidden in the biofilm and mucus double barrier and simultaneously regulate local antifungal immunity enhancement, which may provide a new approach to treat refractory drug-resistant biofilm-associated mucosal candidiasis.

Funding

This study was supported by the Chongqing Natural Science Foundation Project [No. CSTB2022NSCQ-MSX0124], and Chongqing Graduate Student Research Innovation Project [No. CYB22223].

Disclosure

The authors declare no conflicts of interest in this work.

References

1. Hu L, He C, Zeng C, Li X, Hua F, Yan Z. Characterization of oral candidiasis and the Candida species profile in patients with oral mucosal diseases. *Microb Pathog*. 2019;137:103575. doi:10.1016/j.micpath.2019.103575
2. Willems H, Ahmed SS, Liu J, Xu Z, Peters BM. Vulvovaginal candidiasis: a current understanding and burning questions. *J Fungi*. 2020;6(1):27. doi:10.3390/jof6010027
3. Lopes JP, Lionakis MS. Pathogenesis and virulence of Candida albicans. *Virulence*. 2022;13(1):89–121. doi:10.1080/21505594.2021.2019950
4. Chandra J, Kuhn DM, Mukherjee PK, Hoyer LL, McCormick T, Ghannoum MA. Biofilm formation by the fungal pathogen Candida albicans: development, architecture, and drug resistance. *J Bacteriol*. 2001;183(18):5385–5394. doi:10.1128/JB.183.18.5385-5394.2001
5. Muzny CA, Schwebke JR. Biofilms: an underappreciated mechanism of treatment failure and recurrence in vaginal infections. *Clin Infect Dis*. 2015;61(4):601–606. doi:10.1093/cid/civ353
6. Sheng YH, Hasnain SZ. Mucus and mucins: the underappreciated host defence system. *Front Cell Infect Microbiol*. 2022;12:856962. doi:10.3389/fcimb.2022.856962
7. Lock JY, Carlson TL, Carrier RL. Mucus models to evaluate the diffusion of drugs and particles. *Adv Drug Deliv Rev*. 2018;124:34–49. doi:10.1016/j.addr.2017.11.001
8. Witten J, Ribbeck K. The particle in the spider's web: transport through biological hydrogels. *Nanoscale*. 2017;9(24):8080–8095. doi:10.1039/C6NR09736G
9. Forier K, Raemdonck K, De Smedt SC, Demeester J, Coenye T, Braeckmans K. Lipid and polymer nanoparticles for drug delivery to bacterial biofilms. *J Control Release*. 2014;190:607–623. doi:10.1016/j.jconrel.2014.03.055
10. Li P, Chen X, Shen Y, et al. Mucus penetration enhanced lipid polymer nanoparticles improve the eradication rate of Helicobacter pylori biofilm. *J Control Release*. 2019;300:52–63. doi:10.1016/j.jconrel.2019.02.039

11. Xu Q, Ensign LM, Boylan NJ, et al. Impact of Surface Polyethylene Glycol (PEG) density on biodegradable nanoparticle transport in mucus ex vivo and distribution in vivo. *Acs Nano*. 2015;9(9):9217–9227. doi:10.1021/acsnano.5b03876
12. Yang M, Lai SK, Wang YY, et al. Biodegradable nanoparticles composed entirely of safe materials that rapidly penetrate human mucus. *Angew Chem Int Ed Engl*. 2011;50(11):2597–2600. doi:10.1002/anie.201006849
13. Torrado JJ, Serrano DR, Uchegbu IF. The oral delivery of amphotericin B. *Ther Deliv*. 2013;4(1):9–12. doi:10.4155/tde.12.134
14. Cavassin FB, Bau-Carneiro JL, Vilas-Boas RR, Queiroz-Telles F. Sixty years of amphotericin B: an overview of the main antifungal agent used to treat invasive fungal infections. *Infect Dis Ther*. 2021;10(1):115–147. doi:10.1007/s40121-020-00382-7
15. Sims LB, Frieboes HB, Steinbach-Rankins JM. Nanoparticle-mediated drug delivery to treat infections in the female reproductive tract: evaluation of experimental systems and the potential for mathematical modeling. *Int J Nanomed*. 2018;13:2709–2727. doi:10.2147/IJN.S160044
16. Hou Y, Yang M, Li J, et al. The enhancing antifungal effect of AD1 aptamer-functionalized amphotericin B-loaded PLGA-PEG nanoparticles with a low-frequency and low-intensity ultrasound exposure on C. albicans biofilm through targeted effect. *Nanoimpact*. 2021;21:100275. doi:10.1016/j.impact.2020.100275
17. Costley D, Mc EC, Fowley C, et al. Treating cancer with sonodynamic therapy: a review. *Int J Hyperthermia*. 2015;31(2):107–117. doi:10.3109/02656736.2014.992484
18. Wang R, Liu Q, Gao A, et al. Recent developments of sonodynamic therapy in antibacterial application. *Nanoscale*. 2022;14(36):12999–13017. doi:10.1039/D2NR01847K
19. Jain A, Tiwari A, Verma A, Jain SK. Ultrasound-based triggered drug delivery to tumors. *Drug Deliv Transl Res*. 2018;8(1):150–161. doi:10.1007/s13346-017-0448-6
20. Yang M, Cao Y, Zhang Z, et al. Low intensity ultrasound-mediated drug-loaded nanoparticles intravaginal drug delivery: an effective synergistic therapy scheme for treatment of vulvovaginal candidiasis. *J Nanobiotechnol*. 2023;21(1). doi:10.1186/s12951-023-01800
21. Yang M, Xie S, Adhikari VP, Dong Y, Du Y, Li D. The synergistic fungicidal effect of low-frequency and low-intensity ultrasound with amphotericin B-loaded nanoparticles on C. albicans in vitro. *Int J Pharm*. 2018;542(1–2):232–241. doi:10.1016/j.ijpharm.2018.03.033
22. Owen DH, Katz DF. A vaginal fluid simulant. *Contraception*. 1999;59(2):91–95. doi:10.1016/S0010-7824(99)00010-4
23. Cook MT, Brown MB. Polymeric gels for intravaginal drug delivery. *J Control Release*. 2018;270:145–157. doi:10.1016/j.jconrel.2017.12.004
24. Albertini B, Passerini N, Di Sabatino M, Vitali B, Brigidi P, Rodriguez L. Polymer-phospholipid based mucoadhesive microspheres prepared by spray-congealing for the vaginal delivery of econazole nitrate. *Eur J Pharm Sci*. 2009;37(4–5):595–601. doi:10.1016/j.ejps.2008.12.009
25. Dwivedi A, Mujtaba SF, Kushwaha HN, et al. Photosensitizing mechanism and identification of levofloxacin photoproducts at ambient UV radiation. *Photochem Photobiol*. 2012;88(2):344–355. doi:10.1111/j.1751-1097.2011.01068.x
26. Cone RA. Barrier properties of mucus. *Adv Drug Deliv Rev*. 2009;61(2):75–85. doi:10.1016/j.addr.2008.09.008
27. Lai SK, Wang YY, Wirtz D, Hanes J. Micro- and macrorheology of mucus. *Adv Drug Deliv Rev*. 2009;61(2):86–100. doi:10.1016/j.addr.2008.09.012
28. Das NJ, Rocha CM, Goncalves MP, et al. Interactions of microbicide nanoparticles with a simulated vaginal fluid. *Mol Pharm*. 2012;9(11):3347–3356. doi:10.1021/mp300408m
29. Cao B, Lyu X, Wang C, Lu S, Xing D, Hu X. Rational collaborative ablation of bacterial biofilms ignited by physical cavitation and concurrent deep antibiotic release. *Biomaterials*. 2020;262:120341. doi:10.1016/j.biomaterials.2020.120341
30. Miller DL. Overview of experimental studies of biological effects of medical ultrasound caused by gas body activation and inertial cavitation. *Prog Biophys Mol Biol*. 2007;93(1–3):314–330. doi:10.1016/j.pbiomolbio.2006.07.027
31. Valle AA, Nobile CJ. Interactions of microorganisms with host mucins: a focus on Candida albicans. *Fems Microbiol Rev*. 2020;44(5):645–654. doi:10.1093/femsre/fuaa027
32. Zou L, Li X, Huang Y, et al. Raspberry-like gold nanozyme-hybrid liposomes for hypoxia-enhanced biofilm eradication. *Nano Today*. 2023;50:101828. doi:10.1016/j.nantod.2023.101828
33. Flemming HC, Wingender J, Szewzyk U, Steinberg P, Rice SA, Kjelleberg S. Biofilms: an emergent form of bacterial life. *Nat Rev Microbiol*. 2016;14(9):563–575. doi:10.1038/nrmicro.2016.94
34. Hu D, Zou L, Yu W, et al. Relief of biofilm hypoxia using an oxygen nanocarrier: a new paradigm for enhanced antibiotic therapy. *Adv Sci*. 2020;7(12):2000398. doi:10.1002/advs.202000398
35. Roy J, Pandey V, Gupta J, Shekhar H. Antibacterial sonodynamic therapy: current status and future perspectives. *ACS Biomater Sci Eng*. 2021;7(12):5326–5338. doi:10.1021/acsbiomaterials.1c00587
36. Matafonova G, Batoev V. Review on low- and high-frequency sonolytic, sonophotolytic and sonophotochemical processes for inactivating pathogenic microorganisms in aqueous media. *Water Res*. 2019;166:115085. doi:10.1016/j.watres.2019.115085
37. Escoffre JM, Lampompes P, Tardy M, Bouakaz A. New insights on the role of ROS in the mechanisms of sonoporation-mediated gene delivery. *Ultrason Sonochem*. 2020;64:104998. doi:10.1016/j.ultsonch.2020.104998
38. Srinivas US, Tan BWQ, Vellayappan BA, Jeyasekharan AD. ROS and the DNA damage response in cancer. *Redox Biol*. 2019;25:101084. doi:10.1016/j.redox.2018.101084
39. Wu X, Zhang S, Li H, et al. Biofilm formation of Candida albicans facilitates fungal infiltration and persister cell formation in vaginal candidiasis. *Front Microbiol*. 2020;11:1117. doi:10.3389/fmicb.2020.01117
40. Phan QT, Myers CL, Fu Y, et al. Als3 is a Candida albicans invasin that binds to cadherins and induces endocytosis by host cells. *PLoS Biol*. 2007;5(3):e64. doi:10.1371/journal.pbio.0050064
41. Shroff A, Sequeira R, Patel V, Reddy K. Knockout of autophagy gene, ATG5 in mice vaginal cells abrogates cytokine response and pathogen clearance during vaginal infection of Candida albicans. *Cell Immunol*. 2018;324:59–73. doi:10.1016/j.cellimm.2017.12.012
42. Williams DW, Jordan RP, Wei XQ, et al. Interactions of Candida albicans with host epithelial surfaces. *J Oral Microbiol*. 2013;5(1):22434. doi:10.3402/jom.v5i0.22434
43. Ouyang W, Chen S, Liu Z, Wu Y, Li J. Local Th1/Th2 cytokine expression in experimental murine vaginal candidiasis. *J Huazhong Univ Sci Technolog Med Sci*. 2008;28(3):352–355. doi:10.1007/s11596-008-0329-9
44. Gao Q, Zhang J, Chen C, et al. In situ mannosylated nanotrinity-mediated macrophage remodeling combats Candida albicans infection. *Acs Nano*. 2020;14(4):3980–3990. doi:10.1021/acsnano.9b07896

45. Zhou S, Bachem MG, Seufferlein T, Li Y, Gross HJ, Schmelz A. Low intensity pulsed ultrasound accelerates macrophage phagocytosis by a pathway that requires actin polymerization, Rho, and Src/MAPKs activity. *Cell Signal*. 2008;20(4):695–704. doi:10.1016/j.cellsig.2007.12.005
46. Gong M, Huang Y, Feng H, et al. A nanodrug combining CD47 and sonodynamic therapy efficiently inhibits osteosarcoma deterioration. *J Control Release*. 2023;355:68–84. doi:10.1016/j.jconrel.2023.01.038
47. Funes SC, Rios M, Escobar-Vera J, Kalergis AM. Implications of macrophage polarization in autoimmunity. *Immunology*. 2018;154(2):186–195. doi:10.1111/imm.12910